Beamline 7.3.1.1

Magnetic Microscopy, Spectromicroscopy

Antiferromagnetic spin reorientation at the Co/NiO(001) interface observed by XPEEM
Ohldag, H., A. Scholl, F. Nolting, F.U. Hillebrecht, J. Stöhr

Direct imaging of interfacial spins in exchange coupled Co/NiO
Ohldag, H., A. Scholl, T.J. Regan, F. Nolting, J. Lüning, C. Stamm, R.L. White, J. Stöhr

Growth kinetics in ultrathin organic films
Fink, R., Th. Schmidt, U. Groh, E. Umbach

Lateral inhomogeneities and termination in ultrathin block copolymer films
Fink, R., Th. Schmidt, N. Rehse, G. Krausch, I. Koprinarov, H. Ade

Magnetic domain structure in multilayers containing metallic antiferromagnets
Scholl, A., A. Doran, H. Ohldag, J. Stöhr

Magnetic microstructure of thin Fe films on Ge
Ohldag, H., F.U. Hillebrecht

Magnetic switching by spin injection
Stamm, C., S. Andrews, A. Scholl, C.T. Rettner, J.-U. Thiele, J. Stöhr

NEXAFS study of self-assembled FePt nanoparticles
Anders, S., S. Sun, C.B. Murray, J.-U. Thiele, M.F. Toney, B.D. Terris

Observation of microphase segregation in binary polymer brushes
Usov, D., C. Froeck, A. Scholl, S. Minko, M. Stamm

Optimization of PEEM-2 for studies of organic thin film
Morin, C., A.P. Hitchcock, H. Ikeura-Sekiguchi, A. Scholl, A. Doran, K. Kaznacheyev

Perpendicular magnetic anisotropy in $CoPt_3$ (111) films grown on a low energy surface at room temperature
Albrecht, M., M. Maret, A. Maier, F. Treubel, B. Riedlinger, U. Mazur, G. Schatz, S. Anders

Photoemission electron microscopy and x-ray magnetic circular dichroism of $Fe_xNi_{(1-x)}$ thin films on Cu(111)
Sato, Y., T.F. Johnson, S. Chiang, X.D. Zhu, D.P. Land, J.A. Giacomo, F. Nolting, A. Scholl

Soft x-ray absorption spectroscopy of *single* nanocrystals
Nolting, F., J. Rockenberger, J. Lüning, J. Hu, A.P. Alivisatos

Valence-state imaging of mineral micro-intergrowths
Smith, A.D., P.F. Schofield, A. Scholl

Antiferromagnetic Spin Reorientation at the Co/NiO(001) Interface Observed by XPEEM

H. Ohldag[1,2,5], A. Scholl[2], F. Nolting[3], F.U. Hillebrecht[4] and J. Stöhr[1]

[1]Stanford Synchrotron Radiation Laboratory, Stanford University, Stanford, California 94309, USA.
[2]Advanced Light Source, Ernest Orlando Lawrence Berkeley National Laboratory, University of California, Berkeley, California 94720, USA.
[3]Swiss Light Source, Paul Scherrer Institut, 5232 Villingen, Switzerland.
[4]Max Planck Institut für Mikrostrukturphysik, 06120 Halle, Germany.
[5]Institut für Angewandte Physik, Heinrich Heine Universität Düsseldorf, 40225 Düsseldorf, Germany.

BACKGROUND

The exchange bias phenomenon plays a key role in magnetic-device technology, such as the giant magnetoresistance (GMR)-effect read heads. But exactly how exchange bias works is not very well understood. The spin orientation on each side of the antiferromagnet/ferromagnet interface is one of the missing pieces of information. We addressed this issue by studying nickel oxide single crystal exhibiting a (100) oriented surface. Nickel oxide single crystals have been well characterized in the literature and exhibit large antiferromagnetic domains which X-ray Photoemission Electron Microscopy (XPEEM) with a spatial resolution of 50 nm for magnetic structures can easily image using the technique of x-ray magnetic linear dichroism (XMLD). Image contrast arises because the relative orientation of the polarization of the x-ray beam and the magnetic axis in the antiferromagnetic domains influences the shape of the x-ray absorption spectra. To image ferromagnetic cobalt layers, we used x-ray magnetic circular dichroism (XMCD) with circularly polarized light. By employing the surface sensitivity of XPEEM we can then compare our data to the well known bulk data.

RESULTS

The first set of XMLD measurements, made on bare nickel oxide, revealed a complex domain pattern related to that previously known for bulk single crystals, but with some differences. In the bulk, the domains are defined by the (111) crystallographic planes in which the spins lie and the [211] directions in which they are aligned. Analysis of the XPEEM images yielded the same [211] magnetic axes but in a different arrangement. In addition, the XPEEM data showed that some of the boundaries between the domains (domain walls) had decreased magnetic symmetry (Figure 1).

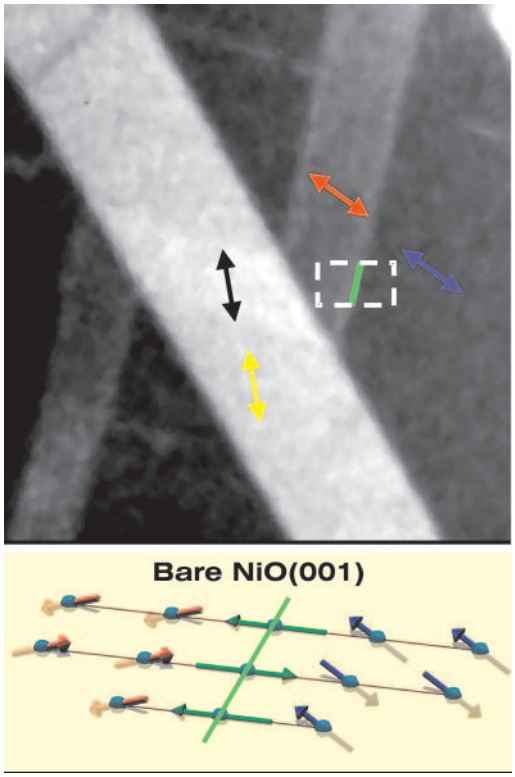

Figure 1: Antiferromagnetic domains on NiO(001)in an area 12 μm across. The colored arrows indicate the projections of the antiferromagnetic axes in the surface plane for four types of domains. Domains with identical in-plane projections (e.g., those marked with red and blue arrows) can be distinguished by examining their orientation out of the surface plane, as illustrated in the sketch at the bottom for the area in the dashed box. The green line represents a domain wall where the spins are in-plane

In a second step we deposited 8 monolayer of ferromagnetic cobalt layer by electron beam evaporation. Upon deposition a reorientation of the nickel spins takes place such that only domains with walls in (100) crystallographic planes remained (Figure 2). Moreover, the spins in the domains assumed [110] directions parallel to the interface. XMCD measurements showed that the magnetization in the cobalt domains was aligned, domain by domain, parallel to the magnetic axes of the nickel oxide domains. Heating the sample to above the Néel temperature destroys the correlation, indicating that the domain pattern observed is indeed caused by exchange coupling between the two systems.

We conclude that a realistic model of exchange bias cannot rely on the bulk structure of the antiferromagnet but has to consider deviations of the spin axis at the interface. These experiments are made possible by the unique combination of chemical, magnetic and surface sensitivity of XPEEM in combination with a tuneable and polarized x-ray source.

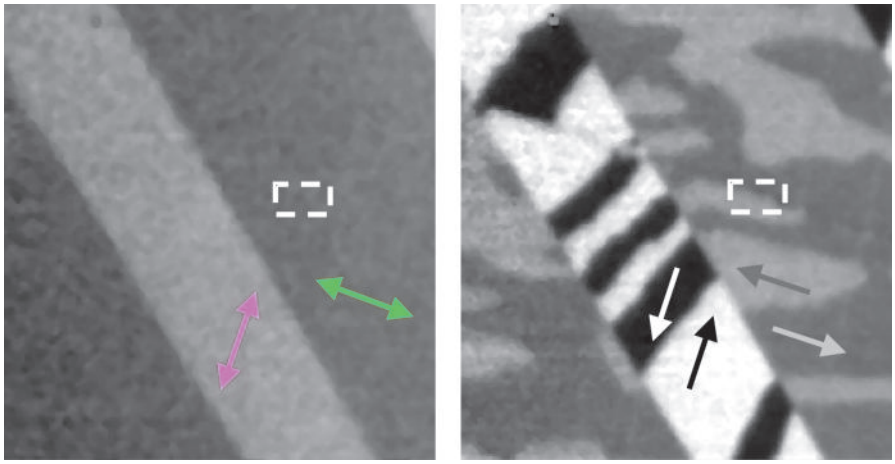

Figure 2: Antiferromagnetic (left) and ferromagnetic (right) domains after deposition of eight monolayers of cobalt. The antiferromagnetic axes have rotated into the surface plane so that only two types of domains can now be distinguished. On top of each antiferromagnetic domain, two ferromagnetic domains can be formed with their magnetization in either of two directions parallel to the antiferromagnetic axis underneath.

References

[1] H. Ohldag, A. Scholl, F. Nolting, S. Anders, F.U. Hillebrecht, and J. Sthr, *"Spin reorientation at the antiferromagnetic NiO(001) surface in response to an adjacent ferromagnet*, Phys. Rev. Lett. **86**, 2878 (2001).

This work was supported by the Director, Office of Basic Energy Sciences of the U.S. Department of Energy. It was carried out at the Advanced Light Source

Principal investigator: Hendrik Ohldag, Stanford Synchrotron Radiation Laboratory, c/o Advanced Light Source, Ernest Orlando Lawrence Berkeley National Laboratory.

Email: hohldag@lbl.gov. Telephone: 510-486-6645.

Direct Imaging of Interfacial Spins in Exchange Coupled Co/NiO

H. Ohldag[1,2,5], A. Scholl[2], T.J. Regan[4], F. Nolting[3], J. Lüning[1], C. Stamm[1], R.L. White[4] and J. Stöhr[1]

[1]Stanford Synchrotron Radiation Laboratory, Stanford University, Stanford, California 94309, USA.
[2]Advanced Light Source, Ernest Orlando Lawrence Berkeley National Laboratory, University of California, Berkeley, California 94720, USA.
[3]Swiss Light Source, Paul Scherrer Institut, 5232 Villingen, Switzerland.
[4]Stanford University, Stanford California 94305, USA.
[5]Institut für Angewandte Physik, Heinrich Heine Universität Düsseldorf, 40225 Düsseldorf, Germany.

BACKGROUND

The determination of the crystallographic, electronic or magnetic structure of interfaces has remained one of the great challenges in all of materials science. The key reason is the difficulty to detect and isolate the weak interface signature from that of the dominant bulk. This is largely due to the lack of depth specificity of most techniques, impeding the detection of a signal from a well-defined depth, only. For lack of better capabilities scientists have tried to circumvent this problem, often studying the early stages of interface formation with surface science techniques or simply assuming "perfect" interfaces between "bulk" materials.

The exchange bias effect, empirically discovered nearly 50 years ago, is used today to create a well-defined ferromagnetic reference layer in a magnetic device. A natural ferromagnet has a preferred magnetization "easy axis", and an external field can align the spins into either of two equally stable directions along this axis - the magnetization loop is symmetric. If an AFM-FM system is grown in a magnetic field or, after growth, is annealed in a magnetic field to temperatures above the AFM Néel temperature, then the FM exhibits a preferred magnetization direction parallel to the applied field. Furthermore its coercivity is usually increased (even without external field applied). The easy alignment direction can serve as a reference direction in a device. It is clear that exchange bias has to originate from the coupling of the spins in the AFM to those in the FM but, because of the magnetic neutrality of the AFM, the coupling has to involve *uncompensated spins* at the AFM-FM interface. The key to the exchange bias puzzle lies in the determination of the origin of these interfacial spins and their role in the magnetic properties of the system. It is the very difficulty associated with the determination of

the magnetic interfacial structure mentioned above, that has impeded the solution of the exchange bias puzzle for more than forty years. X-ray magnetic circular (XMCD) and linear (XMLD) dichroism techniques in conjunction with spectro-microscopy these x-ray techniques now allow a unique fresh look at the old exchange bias problem and hold the promise to finally solving it.

RESULTS

Results were obtained by two complementary experiments, high energy resolution (150 meV)soft x-ray absorption spectroscopy in total electron yield mode performed at Beam Line 10-1 at SSRL and high spatial resolution (50 nm) soft x-ray absorption microscopy using the PEEM2 microscope at the ALS. Figure 1 shows how the spectroscopic knowledge was used to isolate the signal arising from the interfacial spins. The NiO XMLD image at the bottom and the Co XMCD image at the top demonstrate the parallel coupling between antiferromagnet and ferromagnet as it was reported earlier [1]. In addition spectra of pure ferromagnetic Co or Ni metal and pure antiferromagnetic CoO and NiO monoxides are shown. X-ray absorption spectra of thin Co layers (up to 10 monolayer) deposited on NiO deviate significantly from the pure metal and furthermore the deposition leads to a change in the NiO absorption spectra. The changes are interpreted in terms of a chemical process that leads to reduction of NiO to Ni and oxidation of Co to CoO and thus to the formation of a thin $CoNiO_x$ like interfacial layer. Absorption spectra obtained from such systems can be fitted by linear combination of these two single components. The absorption resonances of nickel oxide and metal are slightly different (0.3eV) and by tuning the photon energy appropriately the contribution of metal like Ni sites is enhanced and using circular polarization their ferromagnetic domain pattern can be imaged. This is shown in the middle image of figure 1. A close look on the domain pattern reveals that the domains mimic the antiferromagnetic NiO domains below and the ferromagnetic Co domains above and therefore form the bridge between the two. The absolute number of interfacial spins determined by the size of the ferromagnetic contrast increases with annealing of the sample corroborating the fact that its origin is indeed a chemical reaction. We point out that none of the samples investigated have shown any detectable exchange bias . It is known that exchange bias on single crystals is rather small and scales with the inverse domain size. In contrast the coercivity of the films roughly followed the number of uncompensated spins and could be increased up to 0.15T.

The results show that interfacial spins at the Co/NiO interface are created by a chemical reaction. They are shown to be responsible for the coercivity increase usually observed in AFM-FM exchange coupled systems.

References

[1] H. Ohldag, A. Scholl, F. Nolting, S. Anders, F.U. Hillebrecht, and J. Stöhr, *"Spin reorientation at the antiferromagnetic NiO(001) surface in response to an adjacent ferromagnet*, Phys. Rev. Lett. **86**, 2878 (2001).

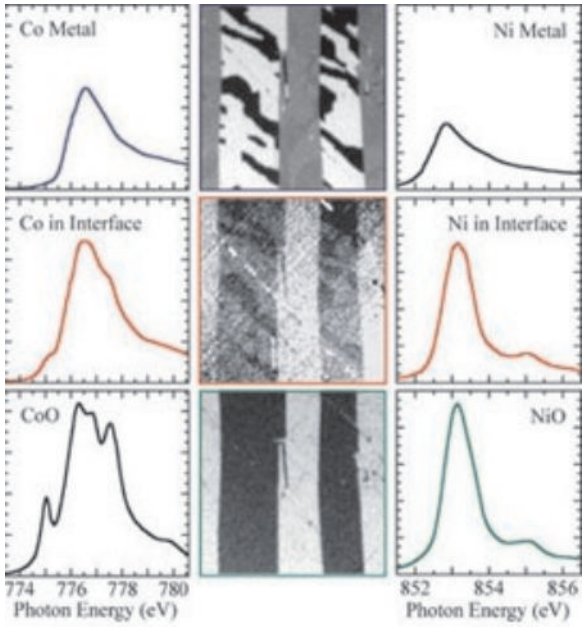

Figure 1: Co (left column) and Ni (right column) high resolution L_3 edge x-ray absorption spectra resolving the fine structure of the metal (top) and the oxide (bottom). The XAS of the Co and Ni atoms in the interfacial layer (middle) reveal a chemical reaction of Co oxidation and Ni reduction. The resulting spectra can be understood as a linear combination of metal and oxide spectra. By choosing appropriate photon energies and polarization x-ray photoemission electron microscopy images (XPEEM) reveal the ferromagnetic domain pattern of Co the antiferromagnetic domain pattern of NiO and the interfacial spin polarization of the interfacial spins (middle).

[2] H. Ohldag, T. J. Regan, J. Stöhr, A. Scholl, F. Nolting, J. Lüning, C. Stamm, S. Anders and R. L. White,*"Spectroscopic identification and direct imaging of interfacial magnetic spins"*, Phys. Rev. Lett. **87**, 247201 (2001).

[3] T. J. Regan, H. Ohldag, C. Stamm, F. Nolting, J. Lüning, J. Stöhr and R. L. White, *"Chemical effects at metal/oxide interfaces studied by x-ray-absorption spectroscopy"*, Phys. Rev. B **64**, 214422 (2001).

This work was supported by the Director, Office of Basic Energy Sciences of the U.S. Department of Energy. It was carried out at the Advanced Light Source and the Stanford Synchrotron Radiation Laboratory.

Principal investigator: Hendrik Ohldag, Stanford Synchrotron Radiation Laboratory, c/o Advanced Light Source, Ernest Orlando Lawrence Berkeley National Laboratory.

Email: hohldag@lbl.gov. Telephone: 510-486-6645.

Growth kinetics in ultrathin organic films

R. Fink, Th. Schmidt, U. Groh, E. Umbach
Experimentelle Physik II, Universität Würzburg, Am Hubland, D-97074 Würzburg, Germany

INTRODUCTION

Thin films of large organic molecules are interesting model systems with respect ot their technological importance. Nowadays, more and more applications of such materials are reported, e.g. in microelectronics, light-emitting devices, or photosensors. However, for many applications, the conventional films prepared by sublimation in high vacuum without control of the structural properties, are polycrystalline with lots of structural defects, which drastically influence the electronic and optical properties of such devices. Structural order becomes even more important in devices, where the formation of well-defined heterointerfaces of organic substances is preferred, e.g., when combining p- and n- conducting organic materials.

Previous experiments have demonstrated the influence of the metal-organic interface on the formation of different superstructures which extend into the third dimension and may lead to ideal epitaxial film growth. However, although polymorphic phases are known for many organic materials, it is difficult to optimize the growth conditions with respect to long-range ordered homogeneous films.

EXPERIMENT AND RESULTS

We have used XPEEM to investigate the film morphologies of ultrathin NTCDA films on Ag(111) for different growth conditions. NTCDA has been chosen since the molecular orientation in thin films can easily be manipulated by variation of the substrate temperature between 200 K and room temperature [1]. The experiments were performed at PEEM2 (BL 7.3.1.1). The Ag substrate was prepared by repeated sputter-annealing cycles. The NTCDA films were grown by vacuum sublimation in a separate preparation chamber. We recorded images for various photon energies to extract local NEXAFS/XANES spectra.

Fig. 1 shows XPEEM images two differently prepared films. The nominal film thickness varies by about 50 per cent for the two samples; the evaporation rate was estimated to about 1 monolayer per minute. Two different growth modes were detected: at elevated temperatures of 320 K the prominent structures are rectangularly shaped dark areas on a bright background. The high emission intensity is due to emission from the Ag substrate which is favored under these conditions for all photon energies, since the secondary electron yield (image formation in XPEEM without energy filter is primarily due to secondaries with low kinetic energy !) for Ag is much larger than for the organic compound. The dark areas are identified as NTCDA microcrystals. A closer inspection of their relative orientation yield angles of 60 and 120 degrees for their long axis. Thus, we may directly conclude that the underlying Ag(111) substrate, which has a 6-fold symmetry (with respect to its top layer) influences the growth direction.

Local NEXAFS spectroscopy clearly yields π^*-resonances characteristic for NTCDA monolayers in a chemisorbed surrounding [2] for areas in between the microcrystals. This indicates a Stranski-Krastanov growth mode, which is consistent with the relatively strong interaction between NTCDA and the metal substrate. LEED investigations reflect the diffraction

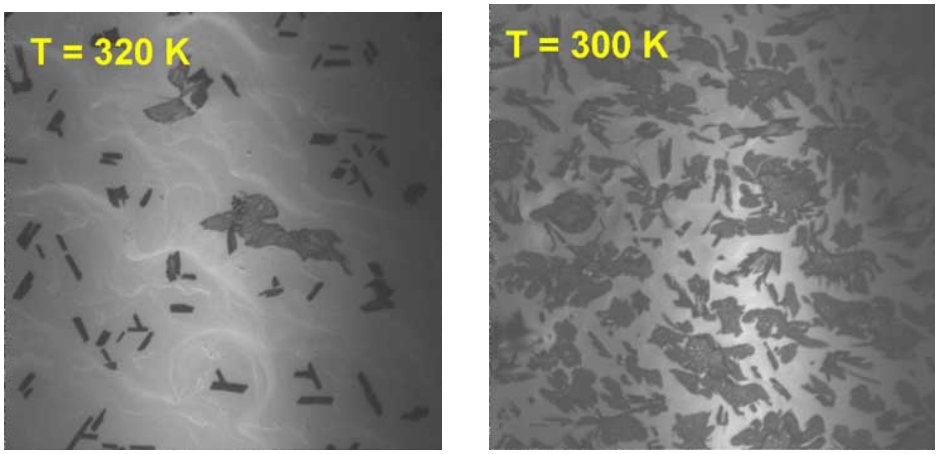

Fig. 1: NTCDA films (nominal thickness around 5 monolayers) adsorbed on Ag(111) at 320 K (left) and 300 K (right). Bright stripes correspond to bunched steps. Image size: 60 x 60 μm², hν = 540 eV.

pattern of the monolayer species (for saturation coverage [3]) and support the finding from the NEXAFSspectra obtained from the bright areas.

For lower temperatures (300 K), the image looks very different. Instead of regularly shaped domains we find fractal growth of organic islands (Fig. 2, right). Compared to the film growth at elevated temperatures there is a much higher density of islands which is due to the smaller diffusion length. In addition, the individual islands are not homogenous. We attribute this finding to the mismatch of the structural parameters. So far, no experimental evidence is found for epitaxial growth of NTCDA/Ag(111). The LEED pattern in this case is diffuse and shows only broad diffraction spots consistent with the small domains. From other experiments (HREELS) there are indications that this film has a different molecular orientation compared to the high- and low-temperature phases, respectively [1].

From the present geometric setup at PEEM2 it is unfortuntely not possible to derive the local molecular orientation from NEXAFS dichroism. Future experiments will focus on in-situ prepared films to investigate the growth kinetics during adsorption and thus allow the investigation of adsorption processes on a real-time scale. Proper image analysis may give direct access to diffusion parameters (diffusion length, activation energies). In this respect, XPEEM will offer new opportunities and thus overcome present limitation by scanning probe or laterally averaging spectroscopic techniques.

REFERENCES

[1] D. Gador, C. Buchberger, R. Fink, and E. Umbach, Europhys. Lett. **41**(2), 213 (1998).

[2] D. Gador, Y. Zou, C. Buchberger, M. Bertram, R. Fink, and E. Umbach, J. Electr. Spectr. Rel. Phenom. **101-103**, 529 (1999).

[3] R. Fink, D. Gador, Y. Zou, E. Umbach, Phys. Rev. B **60,** 2818 (1999).

This work was supported by the Bundesminister für Bildung und Forschung, contracts 05SL8WW18. We gratefully acknowledge experimental support by A. Scholl and A. Doran during the experiments at PEEM2.

Principal investigator: Rainer Fink. Experimentelle Physik II, Universität Würzburg.
Email: raifi@physik.uni-wuerzburg.de Telephone: +49-931-888-5163.

Lateral inhomogeneities and termination in ultrathin block copolymer films

R. Fink[1], Th. Schmidt[1], N. Rehse[2], G. Krausch[2], I. Koprinarov[3], H. Ade[4]

[1]Experimentelle Physik II, Universität Würzburg, Am Hubland, D-97074 Würzburg, Germany
[2]Physikalische Chemie II, Universität Bayreuth, D-95440 Bayreuth, Germany
[3]Brockhouse Institute for Materials Research, McMaster Univ., Hamilton, ON L8S 4M1, Canada
[4]North Carolina State Univ., Dept. Of Physics, Raleigh, NC 27695 , USA

INTRODUCTION

Linear chain-like molecules consisting of blocks of chemically different components (so-called block-copolymers) in many cases form long-range ordered supramolecular structures. The reason for this behavior is the interplay between phase separation of the different components and the molecular unity in the single molecules. The size of the forming structures depends on the size of the molecules and ranges from about 10 to 100 nm. This is usually called "microphase separation" or "micro domain formation". Due to the differences in the surface free energy of the polymers the structure of the micro domains of the surfaces and interfaces can be manipulated. Whereas the structure and morphology of diblock copolymers has been intensely investigated, the investigation of more complex structures (multiblock copolymers, graft polymers, star-like copolymers, etc.) has started only recently.

Recent investigations demonstrate more complex surface and thin film morphologies [1-3]. E.g., an ABC-triblock copolymer consisting of polystyrene (PS), polybutadiene (PB) and polymethylmethacrylate (PMMA), which forms lamellar-like structures in bulk, forms lateral structures at the surface, since the PB-center block (PB) has the lowest surface free energy [4]. To investigate these structures, microscopic techniques with none or only limited spectral sensitivity have been employed so far (atomic force microscopy, scanning electron microscopy, transmission electron microscopy). Although these techniques offer a limited potential to distinguish the polymer blocks, a definite and unambiguous attribution of the respective polymer subunits is still lacking.

EXPERIMENTS

We have used the unprecedented opportunities of high brilliance synchrotron radiation at the Advanced Light Source in particular the installed microspectroscopes (PEEM2 at BL 7.3.1.1 and STXM at BL 7.0.1) to investigate the stoichiometric inhomogeneities in those films within the bulk (STXM) and in the surface-near region (PEEM). Our preliminary experiments have explicitely demonstrated the usefulness of these microspectroscopic techniques.

Fig. 1 shows a STXM image of a thin film consisting of a PS-PB-PMMA triblock copolymer (floated on a 100 nm thick Si_3N_4 membrane) recorded at a photon energy of 293 eV (image size: 60 x 60 μm^2). The lower image shows a cross section along the red bar clearly indicating the distinct film thicknesses in the sample. This finding is in accordance with the lamellar structure which is formed in bulk of those materials. Brighter spots give a clear indication of an additional lateral fine structure within the homogenous areas. The structures in the upper left corner of Fig. 1 are due to partial dewetting of single terraces.

Fig. 2 shows two XPEEM images recorded at the positive and negative slope of the prominent π^*-resonance ($h\nu$ = 286.5 eV) reflecting a distinct contrast reversal which ist due to the different termination of the various terraces, i.e. in one case the terrace consists mainly of the PS species whereas in the other areas PMMA is the prominent species. Images recorded at the O K-edge

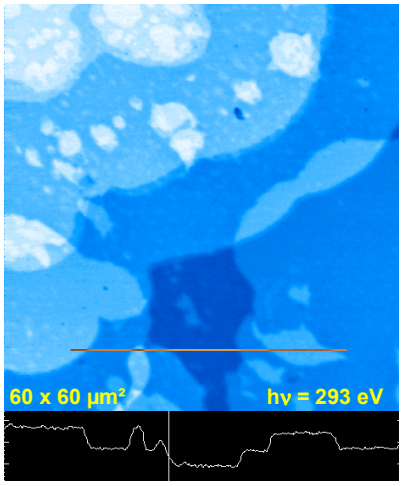

Fig.1: STXM image of a PS-PB-PMMA-triblock copolymerfilm.

allow much higher magnification due to the higher photon flux and thus allow direct imaging of the lateral patterning, which is dominated by the dewetting of the organic film. The finding of differently terminated areas is fully consistent with previous indirect conclusions drawn from AFM data and thus represents a direct spectroscopic proof.

In both cases, PEEM and STXM, the microdomain formation within a terrace with periodicities on the order of up to several 10 nm can at present not be resolved. XPEEM of soft matter films at present is limited to lateral resolutions of about 100 nm and, in addition, may lead to misinterpretations of the spectroscopic data since the high photon flux densities lead to fast degradation/fragmentation of the organic molecules or even conversion into graphite. STXM partly overcomes the latter restriction since the illumination time is significantly shorter. Much higher transmission (by a factor 100 to 1000 at comparable magnification) of the electron optics in an aberration-corrected XPEEM (like, e.g., at PEEM3 or SMART) will improve spectroscopic imaging of surfaces of soft matter films.

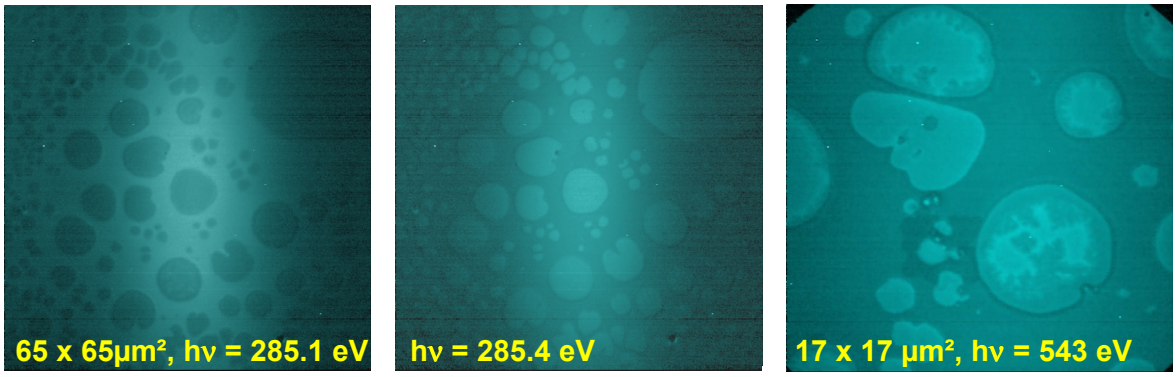

Fig. 2: PEEM images of a PS-PB-PMMA triblock copolymer film indicating the spectroscopic contrast (contrast reversal in the XPEEM images by 0.3 eV photon energy variation). Left and center: excitation at the C K-edge; right:excitation at the O K-edge at higher magnification.Note, that the surface has been plasma-etched to remove the top PB layer.

REFERENCES

[1] W. Stocker, J. Beckmann, R. Stadler, J.P. Rabe, *Macromolecules* **29,** 7502 (1996).

[2] H. Elbs, K. Fukunaga, G, Sauer, R. Stadler, R. Magerle, G. Krausch, *Macromolecules* **32,** 1204 (1999).

[3] K. Fukunaga, H. Elbs, G. Krausch; *Langmuir* **16,** 3474 (2000).

[4] N. Rehse, A. Knoll, R. Magerle, G. Krausch; *Phys. Rev. Lett.* **87.** 035505 (2001)

This work was supported by the Bundesminister für Bildung und Forschung, contracts 05SL8WW18 and 05KS1WCA1. We gratefully acknowledge experimental support by A. Scholl and A. Doran during the experiments at PEEM2. Many thanks to A.P. Hitchcock for providing the AXIS 2000 program for data evaluation.

Principal investigator: Rainer Fink. Experimentelle Physik II, Universität Würzburg.
Email: raifi@physik.uni-wuerzburg.de Telephone: +49-931-888-5163.

Magnetic domain structure in multilayers containing metallic antiferromagnets

Andreas Scholl[1], Andrew Doran[1], Hendrik Ohldag[2], and Joachim Stöhr[2]
[1] Lawrence Berkeley National Laboratory, Berkeley, California 94720, USA
[2]Stanford Synchrotron Radiation Laboratory, P.O. Box 20450, Stanford, California 94309, USA

INTRODUCTION

The magnetic structure of antiferro- and ferromagnetic materials is a very active field of research because of applications in magnetic data storage. Antiferromagnetic layers are an important component of hard disk read heads and of non-volatile magnetic random access memory elements, MRAM. The effect of exchange bias at the interface between an antiferromagnetic (AFM) and a ferromagnetic (FM) layer expresses itself as a unidirectional pinning or anisotropy of the magnetization of the ferromagnet, and is utilized to fix the magnetization in a magnetic reference layer in a spin-valve structure or a magnetic tunnel junction (MTJ), which consists of two ferromagnetic layers separated by a non-magnetic metal (spin-valve) or an insulator (MTJ). Initially, oxide antiferromagnets were used in exchange bias applications but presently metallic alloys of manganese and other transitions metals such as Fe, Ni, Pt or Ir are used because of their larger bias and better stability.

RESULTS

Here we will report recent results on exchange coupling across manganese antiferromagnets, in particular Mn and FeMn thin films. A NiO (001) single crystal was used as substrate material. The crystal was cleaved ex-situ and then prepared by Ar sputtering and subsequent extensive annealing at 800 K in O_2 atmosphere ($1x10^{-6}$ mbar, several hours). LEED images showed a well-ordered surface of cubic symmetry. The same crystal could be reused many times. The ALS PEEM-2 Photoemission Electron Microscope was used to obtain local x-ray absorption spectra and magnetic domain images with magnetic linear and circular dichroism contrast [1,2].

FeMn layers were grown by electron beam evaporation from element sources. The sources were calibrated using a thickness monitor to equal flux in order to grow films of approximately $Fe_{0.5}Mn_{0.5}$ composition. The overview x-ray absorption spectrum in Fig. 1 acquired at low spatial resolution using PEEM shows approximately equal edge jumps at the Mn and Fe edges. The

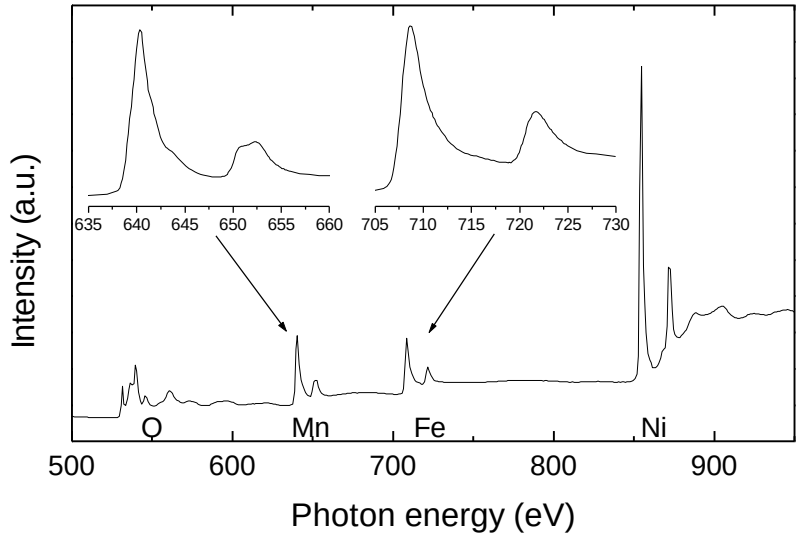

Fig. 1: X-ray absorption spectrum of 13 Å FeMn/NiO acquired by PEEM. The insets show higher resolution spectra of the Mn and Fe edges.

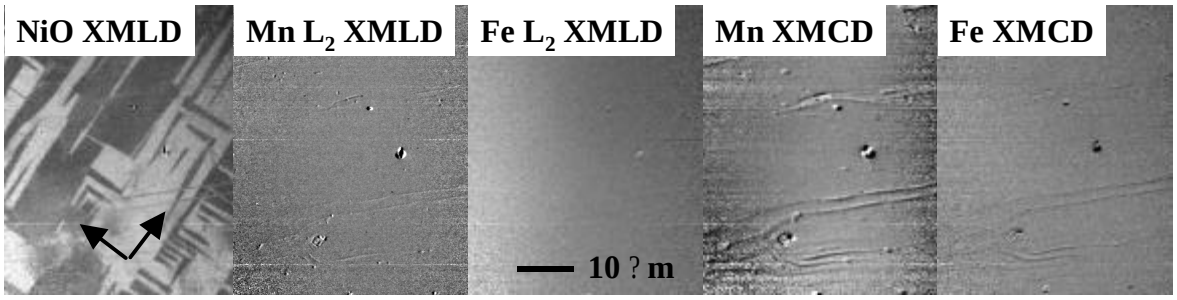

Fig. 2: X-ray magnetic dichroism images of 13 Å FeMn/NiO. Arrows mark the [100] and [010] directions

strong O and Ni signal originates from the NiO substrate. The Mn and Fe edges show the characteristic shapes known for metallic Mn and Fe. In particular, the multiplet structure in the Mn L_3 and L_2 resonance is resolved. No strong oxidization of the FeMn layer is visible in the spectra, which would result in a change of the Fe and Mn line shape.

PEEM magnetic dichroism images using linearly and circularly polarized x-rays show the magnetic domain structure of the NiO substrate and the FeMn thin film, Fig.2. The XMLD image of NiO acquired at the L_2 edge shows the expected domain structure with AFM axes along [110] (vertical, dark color) and [1-10] (horizontal, bright color). Domain walls form along [100] and [010]. The XMLD images acquired at the Mn L_2 edge (see Fig. 1) and at the Fe L_2 edge do not show any discernible contrast within our sensitivity, setting an upper limit for the XMLD contrast in FeMn to 1%. The XMLD contrast in FeMn is therefore much lower as in oxide AFMs, such as NiO or $LaFeO_3$, and thus much more difficult to detect. The non-existent ferromagnetic domain contrast in the Fe and Mn circular dichroism images furthermore proves the non-ferromagnetic, AFM character of the FeMn film. The remaining structure in the images (lines, dots) originates from topography, which is not completely suppressed in the dichroism images.

After growth of 14 Å of pure Fe ferromagnetic domains become visible in the Fe dichroism image. The domain pattern is correlated to the domain pattern in the AFM NiO substrate, Fig.3. The magnetic axes in Fe and NiO couple parallel, indictating a strong uniaxial exchange anisotropy transferred by an AFM FeMn interlayer. For example, black and white domains in the Fe layer belong to domains with a magnetization pointing down or up, respectively. These domains are always located in regions which appear in a dark gray tone in the XMLD image of the buried NiO antiferromagnet and possess a AFM axis which is vertical. The uniaxial coupling across FeMn implies that the magnetic structure in the spacer is similar to the structure in the NiO layer. No correlation should appear if the magnetic structure in the FeMn layer were completely unrelated. Assuming a parallel coupling at the NiO/FeMn interface we deduce that the coupling at the FeMn/Fe interface is parallel as well. These measurements demonstrate how PEEM provides information about the magnetic structure of the metallic AFM interlayer although the domain

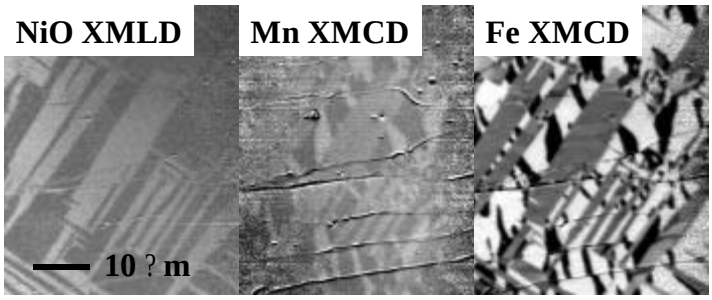

Fig. 3: X-ray magnetic dichroism images of 14 Å Fe/13 Å FeMn/NiO

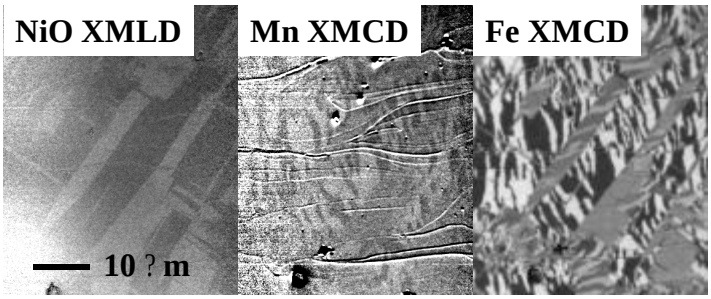

Fig. 4: X-ray magnetic dichroism images of 7 Å Fe/7 Å Mn/NiO

structure is not directly resolved. The XMCD image of Mn in the FeMn layer shows a weak domain contrast which resembles the domain structure in the Fe overlayer, although with opposite sign. Because no contrast was apparent in the Mn XMCD images prior to the growth of pure Fe, we deduce that the appearing contrast is either due to a ferromagnetic polarization of the interface layer, or a chemical reaction at the interface, changing the composition of the interface, a mechanism similar to one observed at oxide-metal interfaces. The inverted contrast shows that Fe and Mn couple antiferromagnetically in the studied sample, a problem that has been discussed controversially in the literature. A possible ferromagnetic moment of the Fe component in the FeMn layer could not be studied because of the large FM signal of the pure Fe layer on top.

A similar behavior was observed in case of pure Mn interlayers. Fig. 4 shows domain images of a 7 Å Fe/8 Å Mn/NiO structure. We again observe a correlation of the magnetic domain patterns across the AFM interlayer. We furthermore observe a ferromagnetic Mn moment. The domain contrast is inverted, demonstrating an antiferromagnetic interface coupling between Fe and Mn. The less regular domain structure in the Fe layer and the appearance of brightness variations within ferromagnetic domains furthermore indicates a weaker coupling across the Mn spacer than across FeMn.

REFERENCES

[1] S. Anders *et al.*, Rev. Sci. Instrum. **70**, 3973 (1999).
[2] A. Scholl et al., Science, 287, 1014 (2000).

This work was supported by the Director, Office of Energy Research, Office of Basic Energy Sciences, Materials Science Division, of the U.S. Department of Energy under Contract No. DE-AC03-76SF00098.

Principal investigator: Andreas Scholl, Lawrence Berkeley National Laboratory. Email: a_scholl@lbl.gov. Telephone: 510-486-4867.

Magnetic Microstructure of Thin Fe Films on Ge.

H. Ohldag[1,2,3], F.U. Hillebrecht[4]

[1]Stanford Synchrotron Radiation Laboratory, Stanford University, Stanford, California 94309, USA.
[2]Advanced Light Source, Ernest Orlando Lawrence Berkeley National Laboratory, University of California, Berkeley, California 94720, USA.
[3]Institut für Angewandte Physik, Heinrich Heine Universität Düsseldorf, 40225 Düsseldorf, Germany.
[4]Max Planck Institut für Mikrostrukturphysik, 06120 Halle, Germany.

Introduction

We investigated the ferromagnetic (FM) domain structure of a 8nm thin Fe film grown on a Ge substrate using the Photoemission Electron Microscope at the ALS. Semiconductor surfaces used as a substrate for magnetic thin films attracted increased interest over the last decade, because of their broad availability and technological relevance. Furthermore they are usually more easy to prepare than for example single crystalline metal surfaces. Our goal is to prepare FM films exhibiting a cubic anisotropy and a moderate FM domain size of the order of a micrometer. The cubic anisotropy would lead to so called 90° domains, FM domains with a perpendicular alignment of their spin directions. These films can then be used as a substrate for antiferromagnetic (AFM) films exchange coupled to the FM substrate. The size of the AFM domains can then be controlled by the size of the FM domains and due to their perpendicular alignment they can be distinguished in our microscope.

Experimental

A Ge substrate was cleaned in water to remove the water soluble surface oxide layer. After introducing the substrate into the ultra high vacuum system ($p < 10^{-9}$mbar the substrate was annealed at 900K for 15 mins to remove adsorbates. An 8nm thick Fe film was then deposited by electron beam evaporation. We imaged the ferromagnetic domain structure employing the X-ray magnetic circular dichroism (XMCD). The XMCD effect of the FM 3d-metals is manifested in a change of intensity ratio at the L_3/L_2 edge. For a given element the ratio is proportional to the degree of circular polarization and the cosine of the angle between spin and helicity. A FM domain map is obtained by acquiring images at each absorption resonance and dividing them by each other. The resulting image is a map of the angle between spin and helicity.

The left column of Figure 1 shows two domain images taken with opposite helicity. The fact that the contrast is reversed between the two images indicates that it is indeed caused by FM domains. We can identify two types of domains separated by walls parallel to the image diagonal. The imbalance between areas covered by the different domains could be caused by residual fields or strain applied to the substrate during evaporation. If we compare the two images, we identify four different grey scales. However, the absolute intensity in each image can be misleading because the images are not normalized to the incoming intensity or to the pre-edge background. To extract quantitative information about XMCD intensity and the spin axes within each domain one needs to acquire local absorption spectra. This is achieved by taking images for subsequent photon energies and analyzing the image intensity in a certain area as it changes with energy afterwards. The resulting spectra are shown on the right side of figure 1. While the spectra in the small domains change drastically between the different helicities, the spectra in the bigger domains do not change very much. We calculate a variation in the L_3 peak intensity of 18% for the small domains which reaches 28% after correction for the degree of polarization (75%) and the angle of incidence 30°. This is the maximum value expected for bulk Fe, and we can conclude that the spin axis in these domains is in the surface plane and collinear with the light vector. The XMCD intensity of the other domains does not change upon reversal of the helicity, so their spin axis needs to be aligned perpendicular to the light vector. For this situation the cosine of the angle between the spin and the helicity does not change. In summary we observe two FM domains with their spin axes including an angle of 90°. If we take these experimental findings into account we can explain the preferred orientation of the walls parallel to the image diagonal. The magnetization vector rotates from one domain to the within the film plane forming a symmetric Néel wall, with the magnetization vector within the wall plane. This type of wall is typically observed for thin films when the film thickness is smaller than the wall width (about 15nm for Fe).

We conclude that Ge can be used as a substrate to grow FM films exhibiting 90° domains. Future studies will show if AFM films can be grown on top of the ferromagnetic film and how the domain size can be influenced.

References

[1] F.U. Hillebrecht, H. Ohldag, N.B. Weber, C. Bethke, U. Mick, M. Weiss and J. Bahrdt, *Magnetic Moments at the Surface of Antiferromagnetic NiO(100)*, Phys. Rev. Lett. **86**(13), pp. 3419 (2001).

[2] H. Ohldag, A. Scholl, F. Nolting, S. Anders, F.U. Hillebrecht and J. Stöhr, *Spin Reorientation at the Antiferromagnetic NiO(001) surface in Response to an Adjacent Ferromagnet*, Phys. Rev. Lett. **86**(13), pp. 2878, (2001).

The authors would like to thank C.F. Bostedt (Lawrence Livermore National Laboratory) for providing the substrate material. This work was supported by the Max Planck Gesellschaft and the U.S. Department of Energy, Office of Basic Energy Sciences.

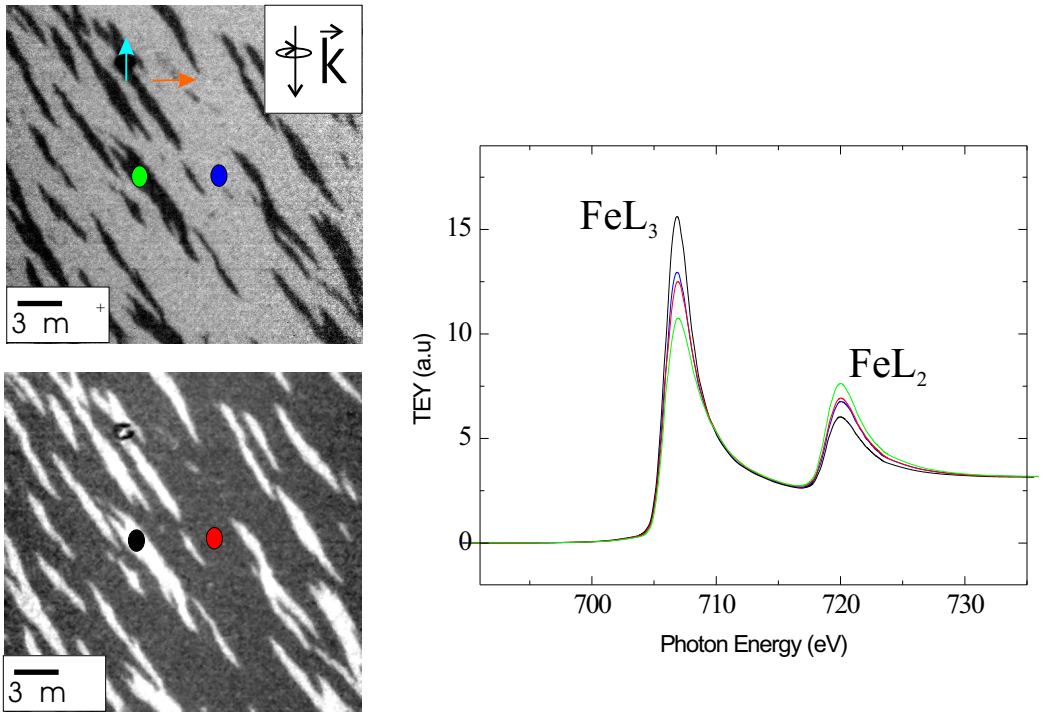

Figure 1: FM domain images taken with opposite helicity are shown on the left. The arrows in the upper image indicate the direction of the magnetization in each domain. The insets denote the dimensions and the helicity of the incoming light. Local x-ray absorption spectra were taken in each of the two domain types and with opposite helicity of the light ($\pm 75\%$ resulting into four spectra. The colored dots in the images correspond to the line color of the spectra. The spectra are shown on the right.

Principal investigator: F.U. Hillebrecht, Max Planck Institut für Mikrostrukturphysik, Weinberg 2, 06120 Halle, Germany. Email: hillebre@mpi-halle.de

Magnetic Switching by Spin Injection

C. Stamm[1], S. Andrews[2], A. Scholl[3], C. T. Rettner[4], J.-U. Thiele[4], J. Stöhr[1]

[1]Stanford Synchrotron Radiation Laboratory, Stanford, CA 94309, USA
[2]Material Science and Engineering, Stanford University, Stanford, CA 94305, USA
[3]Lawrence Berkeley National Laboratory, Berkeley, CA 94720, USA
[4]IBM Almaden Research Center, San Jose, CA 95120, USA

INTRODUCTION

Spin-polarized currents provide a new method of efficiently manipulating nanoscale magnetic domains utilizing the short range and strong electronic exchange interaction. The spins of the injected electrons generate a torque on the magnetization of a ferromagnetic film, which at sufficiently high current densities is capable of switching a magnetic domain. We have started a program to directly observe the magnetic switching process during the spin injection process by means of static and time resolved photoemission electron microscopy utilizing the PEEM-2 microscope on beamline 7.3.1.1.

SAMPLES

One crucial parameter for successful switching by spin injection is a high current density. This can be easily achieved when the current flow is restricted to nano-contacts. In our samples, several 50 nm diameter channels are drilled into a 30 nm thin Si_3N_4 membrane using a focused ion beam. These holes are then filled by copper deposition from both sides, forming nano-contacts. The sample structure and preparation is illustrated in Figure 1.

When a voltage is applied between the front and the back of the membrane, the current has to pass through these nano-contacts. This gives rise to a high current density at the location of the channels, falling off inside the film with distance from the center. A spin polarized current is generated by passing the electrons through a ferromagnetic thin film "polarizer" that is aligned unidirectionally by exchange bias. The "polarizer" is decoupled from a second ferromagnetic thin film "sensor" by a copper interlayer, so the two films are magnetically independent. The micromagnetic configuration of the "sensor" film, which is deposited on top of the structure, is then observed with PEEM-2 as a function of the spin polarized current density.

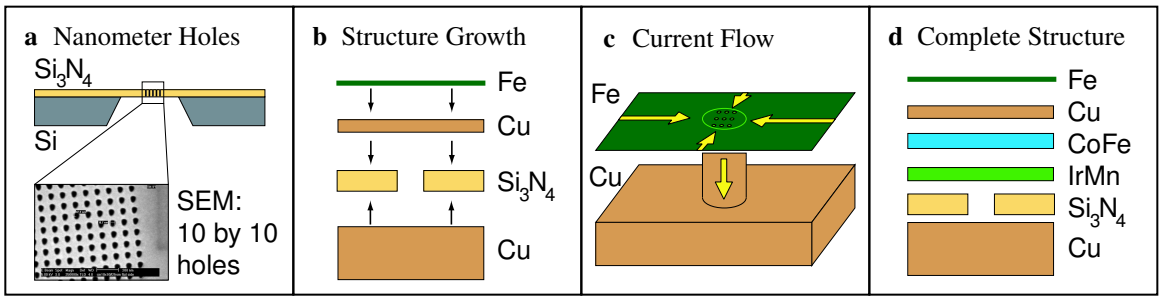

Figure 1: Sample structure for spin injection experiment. **a**: several 50 nm diameter holes are drilled into a Si_3N_4 membrane using a focused ion beam. **b**: Cu is then deposited from both sides, forming nano-contacts. **c**: a current is passed through the Cu filled channels in the membrane and the thin films. **d**: the complete structure, utilizing an exchange biased CoFe/IrMn film as electron polarizer, a Cu buffer layer, and a Fe sensor layer.

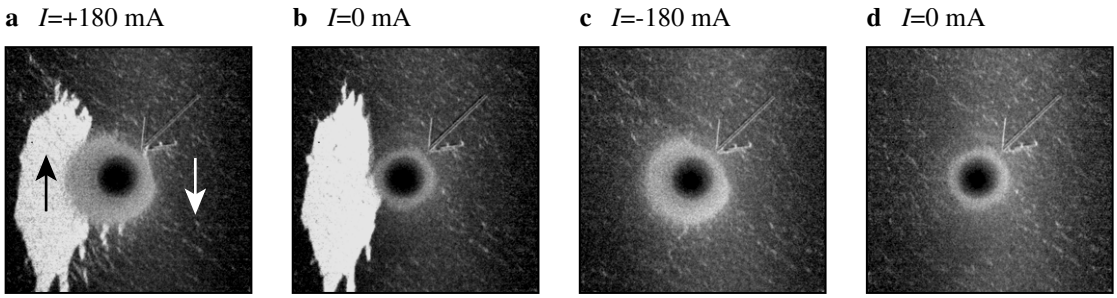

Figure 2: PEEM image at Fe L_3 peak divided by image at Fe L_2 in order to obtain magnetic contrast. The image size is 45 μm. The magnetic axis is along the vertical direction, white corresponds to up and black corresponds to down magnetization (see arrows in **a**). An arrow on the sample points towards the location of the Cu channels. The image series corresponds to different currents through the sample: **a**: the current is able to generate a white domain, which was not present before, it stays when the current is turned off (**b**). **c**, **d**: by reversing the current direction the domain vanishes.

PRELIMINARY RESULTS

First measurements were performed on a sample consisting of Cu channels with a single 8 Å thick magnetic Fe film on top, as shown in Figure 1**b**. A rather large current of up to 180 mA (corresponding to a current density of $j \approx 10^{12}\mathrm{A/m^2}$) was passed through 100 Cu filled channels in the membrane, which destroyed the center region locally (dark circle). However, the measurement demonstrated that the current passes through the Cu channels, and that imaging with PEEM-2 is possible during the injection of a current. The observed switching of a white domain on the left of the channels is due to Oersted-type fields generated by the current. A gray ring around the center region indicates heat generation: the local temperature reached the Curie point, causing loss of magnetic signal.

This work was supported by the Materials Science Division, Office of Basic Energy Sciences of the U.S. Department of Energy.

Contact person:
Christian Stamm, Stanford Synchrotron Radiation Laboratory, M/S 69,
2575 Sand Hill Road, Menlo Park, CA 94025, USA
Email: stamm@slac.stanford.edu, Telephone: 650-926-3042

NEXAFS study of self-assembled FePt nanoparticles

S. Anders[1*], S. Sun[2], C. B. Murray[2], J.-U. Thiele[1], M. F. Toney[1], and B. D. Terris[1]
[1] IBM Almaden Research Center, 650 Harry Road, San Jose, CA 95120
[2] IBM T. J. Watson Research Center, Yorktown Heights, NY 10598

INTRODUCTION

Over the past few years the storage density of magnetic disk drives has increased at a rate of greater than 100% annually. This increase was achieved by scaling the critical physical dimensions, however experiments and theory indicate that there is a limit to this scaling that will be reached within the next few years.
Today's magnetic storage media consist typically of quaternary alloys, e.g. CoCrPtB, with grain sizes in the range of 10-15 nm [1]. The magnetic anisotropy energy E per grain is given by the grain volume V_g and the anisotropy energy density K_u as $E = K_u V_g$. The thermal stability of the grain magnetization can be described by the stability ratio $C = E / k_B T$ where k_B is Boltzman's constant and T the temperature. $C > 60$ [2, 3] is required to store information reliably for 10 years. If we assume cylindrical particles with a height of the typical film thickness of 20 nm and K_u of current media (about $3x10^5$ J/m^3), this implies a minimum stable particle diameter of about 7nm for monodispersed particles.
Since ultimately the transition width is determined by the grain size, higher storage densities require smaller grains. Also, for constant signal to noise, it is desirable to keep the number of grains per bit constant, and thus the grain size is reduced as the density is increased. The grain size distribution for current granular media is very wide with a typical standard deviation for the grain diameter of about σ = 30-35 %. An increase in thermal stability and storage density and a reduction in noise can be achieved by reducing the median grain size with a simultaneous narrowing of the size distribution.
Magnetic nanoparticles [4] can have a very narrow particle size distribution. Here we describe the fabrication and study of magnetic nanoparticles films, and the requirements for their application to magnetic storage.

SELF-ASSEMBLED LAYERS OF MAGNETIC NANOPARTICLES

A possible method to create new magnetic storage media is the deposition of self-assembled layers of magnetic nanoparticles [4] with a very narrow size distribution. In particular we have investigated FePt nanoparticles because the $L1_0$ phase of FePt in thin film form is known to have very high magnetic anisotropy [5]. FePt nanoparticles were prepared by the combination of reduction of $Pt(acac)_2$ (acac=acetylacetonate) and thermal decomposition of $Fe(CO)_5$ or $FeCl_2$ in the presence of oleic acid and oleyl amine. The nanoparticles can be easily dispersed in a variety of solvents. A drop of the solution is placed on the substrate and during the evaporation of the solvent a regular assembly of nanoparticles is formed. The elemental composition of FePt nanoparticle materials is tuned by varying the molar ratio of $Fe(CO)_5$ or $FeCl_2$ and $Pt(acac)_2$.
The FePt particle size can be varied from 3 to 10nm by first growing 3nm monodisperse seed particles *in situ* and then adding more reagents to enlarge the existing seeds to the desired size. The size distribution of the particles is very narrow ($\sigma \leq 5\%$) as can be seen in Figure 1 for a self-assembled layer of 6 nm particles.

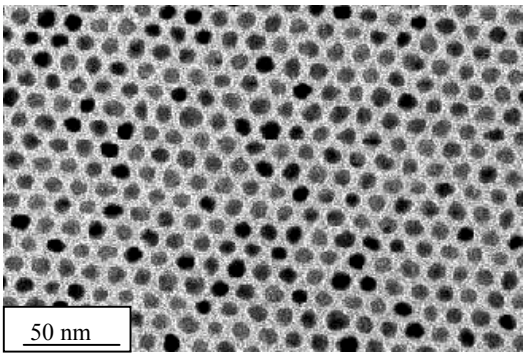

Figure 1: Transmission electron microscope image of self-assembled layer of 6nm diameter FePt nanoparticles.

As deposited, the FePt nanoparticles are in the disordered fcc phase and are superparamagnetic at room temperature. Annealing at various temperatures and durations in nitrogen or forming gas transforms the particles to the ferromagnetic, ordered $L1_0$ phase.

The coercivity of the annealed films typically increases with anneal time and temperature, and a minimum temperature of about 500°C is required to begin forming the ordered $L1_0$ phase. An increased number of layers also leads to an increase in the film coercivity. For magnetic recording thin, high anisotropy layers of small nanoparticles are most desirable. The thinnest layers that showed coercivities > 300 Oe (as measured by Vibrating Sample Magnetometer) were 1 layer films of 8 nm particles and 2 layer films of 4 nm particles. Superconducting quantum interference device (SQUID) measurements show that coercivities as high as 17 kOe can be achieved for 3 layer/4nm particle thin films (deposited from $FeCl_2$ and annealed at 800°C for 5 min. in N_2). The easy axis of the particles is 3D randomly oriented, leading to identical hysteresis loops for in-plane and perpendicular measurements and a remanent magnetization $M_r = 0.5\ M_s$ where M_s is the saturation magnetization.

The chemical nature of the films was studied using near edge X-ray absorption fine structure spectroscopy (NEXAFS) measured in total electron yield at beamline 7.3.1. of the ALS. The data indicate that all films contain a substantial fraction of oxidized Fe. Figure 2 shows an example of the NEXAFS spectra for 1 and 7 layer films of 8 nm particles together with a metallic Fe reference spectrum. One can see that the 7 layer film shows a much more metallic character which is correlated to a much higher coercivity compared to the 1 layer film. The best fit to the experimental data is obtained for a weighted superposition of Fe and Fe_3O_4 reference spectra (55%/45% for 1 layer and 75%/25% for 7 layers) but due to the similarity of the spectra of Fe and FeO and of Fe_3O_4 and Fe_2O_3 we cannot exclude the presence of other oxidation states. The ratio of the contribution of metallic and oxidized iron to the spectra is not identical to the ratio of metallic and oxidized iron in the nanoparticles. We assume a geometry of the nanoparticles with a metallic FePt core surrounded by an oxide shell. The oxide shell will contribute more to the spectrum than the volume fraction of the Fe oxide because of the geometry and the short electron escape depth of only 2-5 nm. The assumption of a metallic core surrounded by an oxide shell is also supported by XRD results. For the 7 layer film of 8 nm particles it was found that 90% of the Fe is present in the ordered $L1_0$ phase. A corresponding oxide shell of only 0.1-0.2 nm thickness is sufficient to produce a 25% contribution to the NEXAFS spectra.

Optimization of annealing conditions and chemistry led to a reduction of the oxidized Fe content and an increase in metallic Fe present in the ordered $L1_0$ phase. Both correlate strongly with increase in the magnetic coercive field.

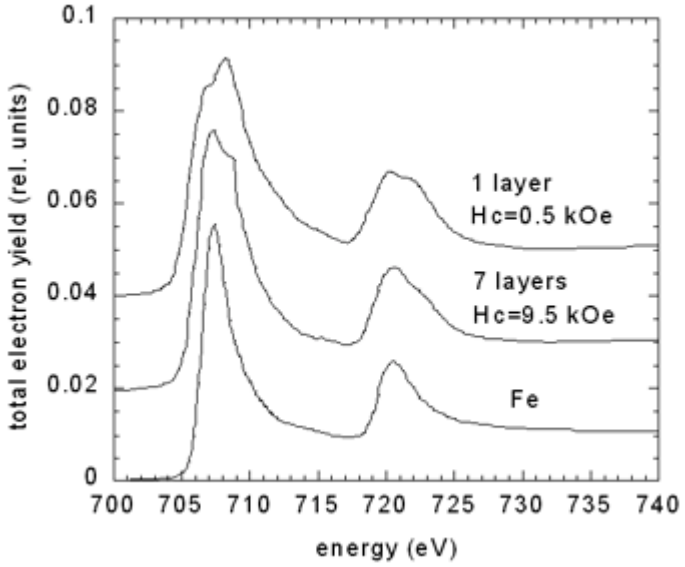

Figure 2: NEXAFS spectra for 1 and 7 layer films of 8 nm particles annealed at 580°C in N_2 for 30 min, together with a metallic Fe reference spectrum. The particles were prepared from $FeCl_2$.

CONCLUSIONS

Thin films of magnetic nanoparticles were investigated as potential candidates for high density magnetic storage media because they exhibit a very narrow size distribution and ultimately the potential of storing one bit per nanoparticle. NEXAFS showed that a fraction of the iron is oxidized, most likely in the form of Fe_3O_4. By optimizing the chemistry and anneal conditions we were able to produce very thin (1 layer/8 nm particles and 2 layers/4nm particles) ferromagnetic films with coercivities of > 300 Oe. Thicker films (3 layers/4nm particles) can have coercivities of up to 17 kOe. Further optimization is required to reach the goal of magnetic storage in the density range of 100 Gb/in^2 and above.

ACKNOWLEDGMENTS

The authors would like to thank Andreas Scholl, Andrew Doran, and Hendrik Ohldag for their ongoing support of their work at the ALS. This work was supported by IBM.

REFERENCES

[1] Y. Kubota, L. Folks, and E. Marinero, J. Appl. Phys. 84 (1998) 6202-7.
[2] S. H. Charap, P.-L. Lu, and Y. He, IEEE Trans. Magn. 33 (1997) 978-83.
[3] D. Weller and A. Moser, IEEE Trans. Magn. 35 (1999) 4423-39.
[4] S. Sun, C. B. Murray, D. Weller, L. Folks, and A. Moser, Science 287 (2000) 1989-92.
[5] D. Weller, A. Moser, L. Folks, M.E. Best, W. Lee, M. Toney, M. Schwieckert, J.-U. Thiele, and M.F. Doerner, IEEE Trans. Magn. 36 (2000) 10-15.

Principal investigator: Simone Anders, IBM Almaden Research Center, 650 Harry Road, San Jose CA 95120.
Email: simone@almaden.ibm.com. Telephone: 408-927-2069.

Observation of microphase segregation in binary polymer brushes

D. Usov[1], C. Froeck[1], A. Scholl[2], S. Minko[1], M. Stamm[1]
[1]Institut for Polymer Research Dresden, Hohe St. 6, 01069 Dresden, Germany
[2]Advanced Light Source, Ernest Orlando Lawrence Berkeley National Laboratory,
University of California, Berkeley, California 94720, USA

INTRODUCTION

The basic idea is creation of smart polymer layers with switching properties such as wetting behavior, adhesion, interaction with biological objects, and permeability of membranes. Such polymer layers can find their application in many areas such as information recording, sensors, self-cleaning clothes covering, nanodevices, in medicine and biological science for mimicking living cell membranes, for selective adsorption and recognition of proteins and living cells. The route, how to make this dream true, comprises binding to solid substrate different polymers[1] or block-copolymers and switch the film structure in such a way, that this film responding to various external stimuli can adopt particular desired properties: hydrophylic/hydrophobic balance, selective adsorption of particular molecules, etc.

We are currently studying model layers composed of two different (hydrophilic and hydrophobic) linear polymers covalently grafted to silicon substrates which can be switched upon exposure to solvents of different thermodynamical quality[1]. The grafting density is so high that the distance between grafting points of neighbor polymer molecules is much (about 10 times) shorter than the size of the polymer coils (mean distance between chain ends in theta-conditions). Therefore the polymer coils interact with their neighbors and are elongated in the direction perpendicular to the substrate. All the conformational changes are cooperative. Such regime is known as the brush regime. If such a binary polymer brush is exposed to a selective solvent which good for the first brush polymer and poor for the second one the first polymer swells and occupies the top layer while the second polymer collapses and occupies the bottom layer near the substrate. If the solvent is replaced by another one with opposite selectivity the brush passes to a state inverse with respect to the previous one. In a solvent good for both polymers they both are present on the top of the layer. The time of solvent evaporation upon drying by nitrogen flow is much smaller than the time for morphology transformation. The morphologies after treatment in a particular solvent are reproducible and reversibly switch upon changing the solvent. We made the assumption that the spacial distribution of the polymers in the dry state after exposition to a solvent is a fingerprint of their distribution under the solvent[2].

The polymers are usually incompatible but only microphase segregation takes place because each polymer chain is chemically bound to a substrate with one end. The size of the aggregates is limited by the chains` length. Two limiting types of morphologies can be distinguished: the layered phase with only perpendicular phase segregation and the “ripple” phase with lateral segregation. Analytical studies of the microphase segregation in binary brushes under melt conditions and in various solvent conditions were done. Self consistent field calculations made by Marcus Müller[2] predict for binary polymer brushes in a solvent good for both components existence of the “ripple” phase consisting of parallel lying cylinders with alternating enrichment by each brush component. For the case of a selective solvent an existence of the “dimple” phase is predicted where the worse soluble polymer forms round clusters and the other polymer occupies the area around them. Experimental observation of microphase segregation in binary

polymer brushes was performed using facilities of the Ernest Orlando Lawrence Berkeley National Laboratory and was briefly reported elsewhere[2].

RESULTS

We synthesized binary polymer brushes by radical polymerization on a Si surface using for the grafting of the second polymer the residual azo-initiator on the surface[1]. The brush components were polystyrene with 25% of fully fluorinated aromatic rings (P(S-co-FS)) and polymethylmethacrylate (PMMA).

We observed the reversible morphology switching from elongated species after treatment in toluene to round clusters after exposition to acetone with Atomic Force Microscopy (AFM) (see Fig.1).

We investigated the chemical composition of the brushes` top layers (≤5 nm) after exposition to toluene and acetone applying X-Ray Photoelectron Emission Microscopy (XPEEM). The difference between the carbon peaks in Near Edge X-Ray Absorption Fine Structure spectra (NEXAFS) for polystyrene (286.1 eV) and PMMA (289.3 eV)[3] was used to distinguish between the polymers. We observed the inverse contrast of elongated species at the XPEEM images recorded at 286.1 eV and 289.3 eV for the brush exposed to toluene (see Fig.2). We were unable to find any chemical contrast at the XPEEM images for the brush exposed to acetone due to a strong signal distortion caused by highly rough brush surface.

The integral NEXAFS spectra were recorded from the surfaces of the brushes after exposure to toluene, acetone, and after annealing at 150ºC for 24 hours in vacuum. The water contact angle on the same surfaces was measured. The chemical composition of the top layers of the brushes was calculated and similar results were obtained from these two methods. The top layer of the brushes was enriched with P(S-co-FS) after exposition to toluene and after annealing and with PMMA after exposition to acetone (see Table 1).

We conclude qualitative agreement of the experimentally observed morphologies with the self consistent field calculations.

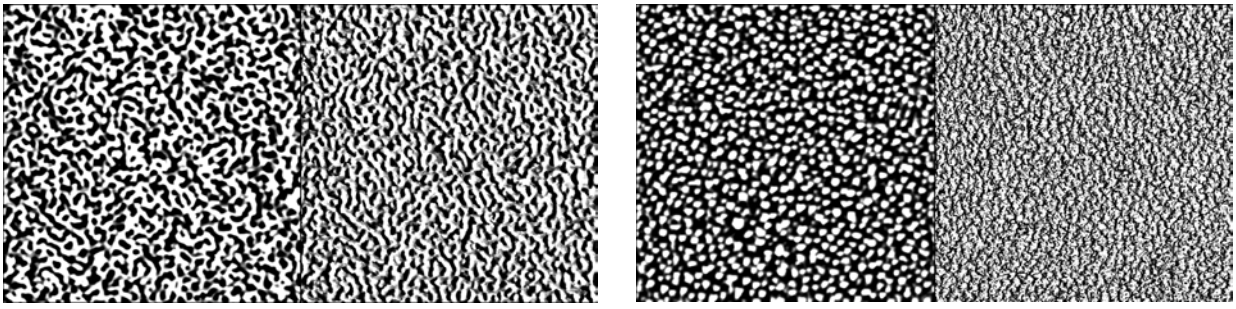

Figure 1. AFM tapping mode images 5x5 μm of the P(S-co-FS)/PMMA brush after exposure to toluene (A,B) and acetone (C,D): topography (A,C), phase (B,D) at 50% set-point ratio.

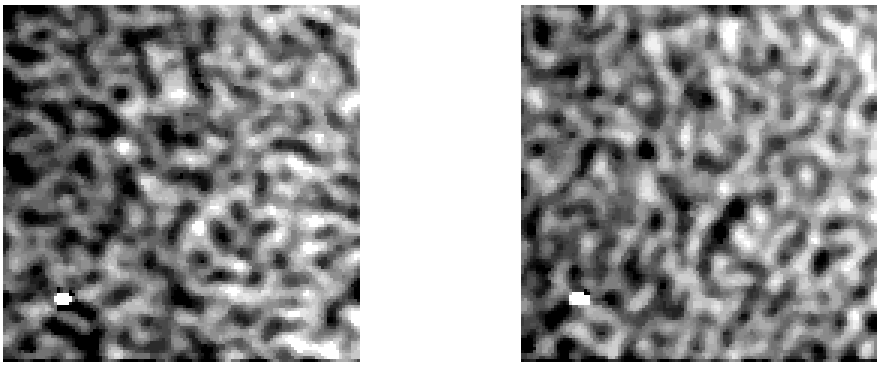

A B

Figure 2. XPEEM images 3x3 μm of the PSF-PMMA1 brush after exposure to toluene showing contrast between C edges of both polymers at 286,1 eV (A) and 289,2 eV (B) for PS and PMMA, respectively.

Table 1. Fraction of PMMA in the top layer of the brushes after exposure to solvents and annealing.

Sample	Contact angle, deg	PMMA fraction in the top layer, % calculated from the contact angle	PMMA fraction in the top layer, % calculated from the XPEEM data
P(S-co-FS)	96.6	0	0
PMMA	76.1	100	100
P(S-co-FS)/PMMA brushes after:			
exposure to toluene	90	32	29
exposure to acetone	81	76	78
in vacuum, at 150°C for 10h	91.5	25	20

REFERENCES

1. Alexander Sidorenko, Sergiy Minko, Karin Schenk-Meuser, Heinz Duschner, and Manfred Stamm, *Langmuir*, Vol. 15, N 24, **1999**, p. 8349.
2. S. Minko, M. Müller, D. Usov, A. Scholl, C. Froeck, and M. Stamm, *Physical Review Letters*, Vol. 88, N 3, **2002**, 035502.
3. Adam Hitchcock, McMaster University, 1280 Main Street West, Hamilton, Ontario, L8S 4L8, Canada, E-mail: aph@mcmaster.ca, private communication.

This work was supported by the Institute for Polymer Research Dresden, Hohe St. 6, 01069 Dresden, Germany and the European Graduate College "Advanced Polymeric Materials", Technical University Dresden, 01062 Dresden, Germany.

Principal investigator: Manfred Stamm, Institute for Polymer Research Dresden, Hohe St. 6, 01069 Dresden, Germany, E-mail: stamm@ipfdd.de, tel. +49 (351) 4658 224, web site: www.ipfdd.de.

Optimization of PEEM-2 for studies of organic thin films

C. Morin[1], A.P. Hitchcock[1], H. Ikeura-Sekiguchi[1,2], A. Scholl[3], A. Doran,[3] K. Kaznacheyev[4]
[1]BIMR, McMaster University, Hamilton, ON, Canada L8S 4M1
[2]Quantum Radiation Division, Advanced Industrial Science and Technology (AIST), Tsukuba, 305-8568 JAPAN
[3]Advanced Light Source, Berkeley Lab, Berkeley, CA 94720
[4]Physics, CLS, University of Saskatchewan, Saskatoon, SK Canada S7N 5C6

INTRODUCTION

There are many potential applications of X-ray photoelectron emission microscopy (X-PEEM) to organic thin films, such as fundamental studies of phase separation [1], and applied studies of organic light emitting diodes, adhesion promoters [2] etc. In order to obtain meaningful results, it is important to unders tand the challenges of applying X-PEEM to organics, and to develop compensating data acquisition strategies. These challenges include: radiation damage, camera artifacts, Io determination, higher order radiation, charging, sample damage from field emission or discharges.

The photon flux at BL 7.3.1 ($>10^{12}$ photons/s at 500 eV in a 30x300 μm spot, with 1.9 GeV, 400 mA) is very high because there are only two optical elements and energy resolution is sacrificed for flux. The high flux, combined with a relati vely inefficient electrostatic column (~5 % transmission at high spatial resolution – 12 μm aperture) and an inefficient camera, mean that ratio of detected signal to number of photons absorbed in the near surface region is very small. In order to perform useful chemical analysis , images of the region of interest must be recorded at a number of energies (in the C1s, N1s or O1s regions for organic samples) to form an image sequence which can be subsequently analysed to obtain point or region spectra, or chem ical maps. Other problems occur because of limitations of the CCD camera - bad pixels; pixel-to-pixel variation in dark signal (leakage) and gain; as well as a slow data transfer rate (0.25s/image, no ability to transfer sub images). A further challenge is the uneven illumination in the PEEM; in order to gain sensitivity we use reduced magnification. Typically the camera views 60x60 μm^2 but only the central third of the image is illuminated.

In order to reduce the damage rate we work at much reduced flux, achieved by placing an aperture (formed by two independently adjustable elements, called ‘ chopper’ and ‘ mask’) in the beam before the monochromator. This reduces the energy resolution as well as the flux – at a chopper value of 15 the resolving power is only 100. Under typical low dose conditions we work with less than 10% of the dynamic range of the camera. Background and camera corrections are extremely challenging. It is essential to record Io spectra from a suitable reference surface, typically HF-etched silicon for organic thin film samples deposited on Si or Si_3N_4. This is especially true in the C 1s region where there is a lot of structure in the Io spectrum. The Io signal must be measured under very similar conditions to those used to study the sa mple in order to ensure the same sensitivity, energy resolution and higher order content, (the latter two depend on the exact choice of chopper, windows, slits and filters used). The PEEM sensitivity is very dependent on the sample-objective lens distance , which changes every time a sample is re-positioned.

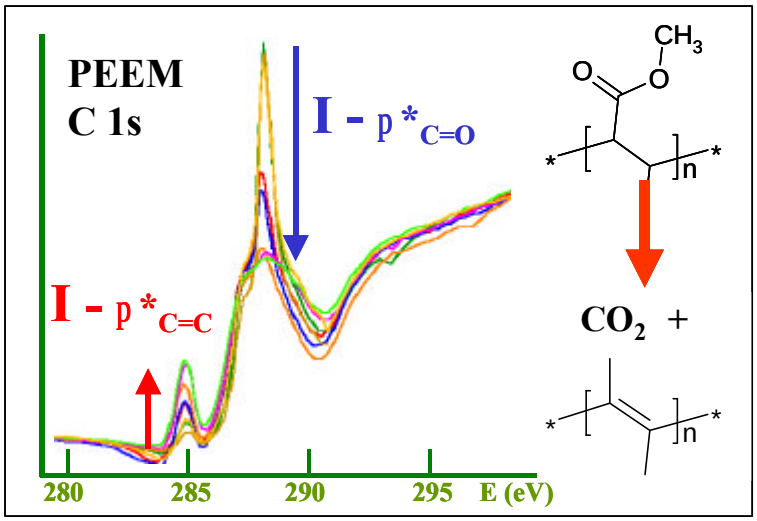

Fig. 1 Plots of C 1s NEXAFS of a 50 nm PMMA film on c-Si. Successive scans made on the same spot build up dose and damage.

Charging can occur for any insulating sample, although it is often surprising the samples that can be studied by PEEM. We typically observe charging if a polymer sample is too thick (> 75 nm), or too corrugated (> 15 nm rms). In some cases a thin metal coating (<2-3 nm) can be evaporated to control charging. Charging results in dark spots on images, where the electrons are trapped by the surface charge potential, or in bright spots, where there is artificially enhanced emission by discharges or, at locations of high curvature, by enhanced detection

probability due to stronger fields. While it is sometimes possible to record meaningful NEXAFS spectra from charging surfaces, more typically, charging resu lts in large and variable sample or objective lens currents which lead to unstable operation, and, in extreme cases, macroscopic discharges that can damage samples, making dramatic dendritic patterns in organic layers, and exploding Si_3N_4 windows. In the following we describe a systematic study of a pure polymethylmethacrylate (PMMA) film in order to characterize its radiation damage rate, and thereby develop procedures to study heterogeneous samples containing PMMA in a meaningful fashion, despite these ch allenges. A detailed manual for operating X -PEEM and choosing parameters optimal for radiation sensitive samples is available at the beam line or from the authors [3].

EXPERIMENTAL

~50 µl of a 1.0% w/w toluene solution of PMMA (Mw = 112.3 K, Mw/Mn = 1.09, Polymer Source Inc) was passed through a teflon filter to remove particulate impurities and dropped onto a spinning HF-etched Si chip at 4000 rpm. Spinning was continued for ~5 s. The film thickness was estimated to be ~40 nm from AFM at a scratch and the rms roughness was 6 nm The sample was not annealed.

Property	Value	Property	Value
Mask	0.9	Dwell (s)	3
Chopper	15 or 16	Camera gain	normal, x8
Al window #1	in	PEEM aperture (µm)	50
Al window #2	in	Sample (kV)	18.0
Exit slit	in	Objective (kV)	13.68
Ti filter (150 nm)	in	Transfer (kV)	12.45
Flash light	on	Intermediate	13.78
Background (Hz)	50	Projection	0

The relationship of measured intensity to the various parameters controlling the signal is summarized in **equation 1**. A number of scale fa ctors need to be determined but this qualitative formula may be useful for others using PEEM-2 for organic thin film studies.

$$S = G*t*[I*\sigma*f_{esc}*F*\varepsilon_{PEEM} - B] \quad \text{(eqn 1a)}$$

where S = detected signal , G = camera gain (2,4,8), t = time, σ = cross-section, f_{esc} = electron escape probability (integrated over inelastic scattering and angular effects), F = work function, ε_{PEEM} = PEEM column efficiency [α (magnification)* (aperture)^2], B = no-X-ray background, and I is the flux (ph/s) on the sample, given by

$$I \alpha\ I_{ring}*C*T \quad \text{(eqn 1b)}$$

where C, the chopper factor is $(C_{max}-C)/C_{max}$; and T, the Ti filter factor, is $(T_{max}-T)/T_{max}$.

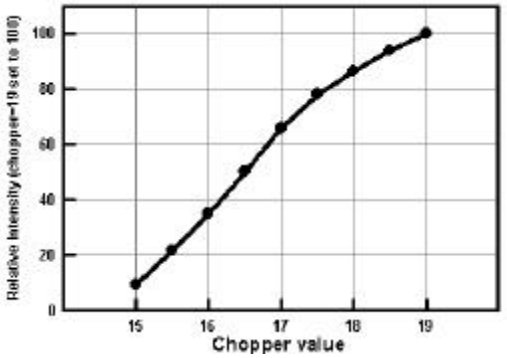

Fig. 2 Variation of flux on sample vs. chopper.

RESULTS AND DISCUSSION

Fig. 1 shows a typical sequence of spectra (without Io correction) recorded while the sample was being damaged. The relative radiation damage rate for PMMA in the low dose regime was determined by recording successive image sequences on the same spot, using the instrumental parameters listed in table 1. Only 24 energies in 283-295 eV range were used in order to track damage changes adequately. In general keeping the number of sampled energies to the minimum is a key step in making meaningful measurements of organics. The *relative dose* was obtained from the integrated spectral signal up to a given measurement, taking into account the dead time between images (~2 s). The *relative damage* was obtained from the increase in the area of the 285 eV $\pi^*_{C=C}$ peak (growth of reduced sites in the backbone) and decrease in the ar ea of the 288 eV $\pi^*_{C=O}$ peak (loss of acrylate groups). In addition to the measurements made at low dose, another series at much higher dose (5 or 10 s exposure at chopper 19) was performed. The two sets were matched in the overlapping region of the 285 eV and 288 eV damage curves. Finally the dose scale was expressed in terms of time equivalent at full flux in the carbon 1s region using the variation of signal strength with chopper setting to scale the times (**Fig. 2**).

Fig. 3 plots damage versus relative dose for PMMA as measured in the PEEM As is typical in radiation damage curves, there is an exponential change with saturation. Based on these results, we estimate that, at the full flux dose rate (chopper = 19, 400 mA in the ALS), the total acceptable exposure time for meaningful measurements of samples containing PMMA with negligible damage (as measured by spectral change) is 10 seconds. Since it takes about 5 seconds to record an image of acceptable quality, if full flux is used it is only possible t o record a few images before the PMMA in a PMMA -containing sample is irreversibly modified. We note that a recent study of radiation damage in various polymers by STXM [4] indicates that PMMA is about average in terms of radiation sensitivity.

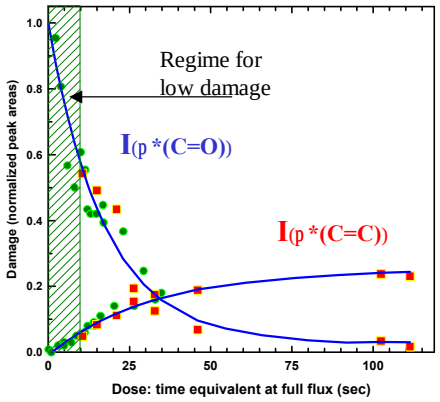

Fig. 3 Intensity at 288 eV and 285 eV versus accumulated radiation dose. The dose is time to equivalent deposited energy when PEEM is operated with full flux. The green points are measurements made at reduced flux. Chopper: green (15), red (19).

Chemical imaging with PEEM requires images at a number of energies.Typically 10 -15 images are needed. The only way to get these without "frying the sample" is to "turn down the torch". We routinely do this by using the chopper to reduce the flux ~10-fold (see Fig. 2). This allows 10-20 images to be recorded prior to significant damage. Chopper values below 15 are not useable since the grating is inadequately illuminated. 2 -bunch mode is also useful, but normalizing the rapid time variation of flux is a challenge.

Fig. 4 presents results of a low dose study of a 20:80 (w/w) PS:PMMA film (PS = polystyrene) which has domain sizes on the order of 250 nm as determined by prior AFM measurements. This is a continuation of our earlier studies of phase segregation on PS:PMMA blends [1]. We are trying to develop a metastable system with flat, reasonably large domains that are pure PS and PMMA, in order to carry out competitive protein adsorption studies. As the analysis of the spectrum of the PMMA -rich regions shows, the as-made material still contains significant PS, as found earlier [1]. However, with our refined understanding of the damage rate of PMMA in PEEM-2, we are now very confident that the 285 eV signal observed in the PMMA -rich domains is from incompletely phase segregated PS and NOT from the C=C bonds formed from radiation damage of PMMA (Fig 1).

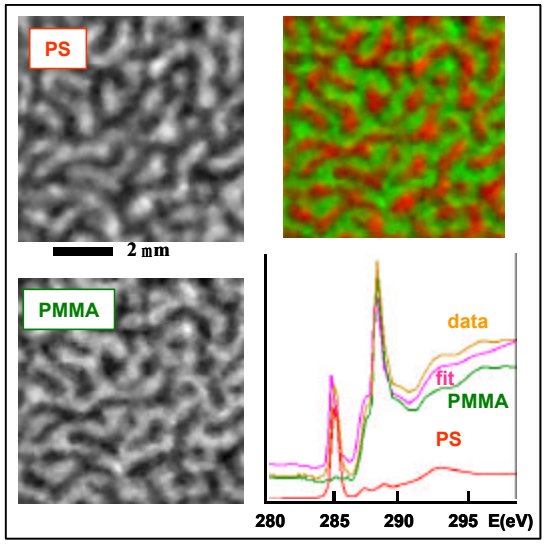

Fig. 4 PS and PMMA component maps, and color composite derived from image sequence of as -made 20:80 PS:PMMA blend, using low dose protocol (3s dwell, chopper=16, few points). Lower right shows the results of a curve fit to the spectrum of pixels in strong PMMA regions. (Jun-01).

SUMMARY: Relative dose - damage relationships for PMMA were measured in PEEM-2 to define an acceptable regime [5]. Similar calibration measurements are required prio r to study of other radiation sensitive samples. Self-assembled monolayer and micro -contact printed systems involving fluorocarbons are particularly challenging due to their very small thickness (< 5nm) and extreme radiation sensitivity. An even more rigorous application of the methods outlined in this report is required for successful studies of such materials.

1. C. Morin et al, *J. Electron Spectrosc* 121 (2001) 203-224
2. G. E. Mitchell, et al. 1999 ALS Compendium (2000)
3. C. Morin, A.P. Hitchcock, H. Ikeura-Sekiguchi, A. Doran and A. Scholl, PEEM -2 manual (2001).
4. T. Coffey, S.G. Urquhart and H. Ade, *J. Electron Spectroscopy* 122 (2002) 65.
5. C. Morin, A.P. Hitchcock, et al in preparation.

Supported by NSERC (Canada) and Canada Research Chair program. ALS is supported by U.S. DoE (DE-FG02-89ER60858). Data analysis done with **aXis2000**, an IDL widget available at http://unicorn.mcmaster.ca/aXis2000.html

Principal investigator: *Adam Hitchcock*, McMaster, aph@mcmaster.ca. Ph: 905 525-9140

Perpendicular magnetic anisotropy in $CoPt_3$ (111) films grown on a low energy surface at room temperature

M. Albrecht[1], M. Maret[1], A. Maier[1], F. Treubel[1],
B. Riedlinger[1], U. Mazur[1], G. Schatz [1], and S. Anders[2]
[1]University of Konstanz, Department of Physics, P.O. Box M621, D-78457 Konstanz, Germany
[2]IBM Almaden Research Center, 650 Harry Road, San Jose, CA 95120

INTRODUCTION

Co-Pt binary alloys have been extensively studied. Owing to their strong perpendicular magnetic anisotropy (PMA) they are potential materials for high-density magneto-optical recording [1, 2]. In fcc $Co_xPt_{\{1-x\}}$ films PMA has various causes such as growth-induced heterogeneity, compressive strain, short-range order driven by surface segregation, or magnetically induced phase separation, but it is not linked to the appearance of any chemical long-range ordered phase. The ordered $CoPt_3$ phase ($L1_2$-type) which can be regarded as a chemically ordered fcc structure with Co atoms at the cube corners and Pt atoms at the face centers in the atomic unit cell shows no PMA due to its cubic symmetry. This is also true for the chemically disordered phase where the Co and Pt atoms are randomly distributed on the fcc lattice. Nevertheless, it was previously reported that epitaxial $CoPt_3$(111) films grown on Pt(111) and Ru(0001) at temperatures between 200-400°C exhibit strong PMA and large coercivities as well as no chemical long-range ordering (LRO) [3, 4]. These observations can be explained by structural short-range ordering effects.
We have recently reported [5, 6] that $CoPt_3$(111) films grown on a van der Waals surface of WSe_2(0001) exhibit remarkable properties: strong PMA for deposition temperatures $T_g < 150$°C and the appearance of chemical long-range ordering ($L1_2$-type) at a deposition temperature of about 100°C, which is 400°C lower than observed for $CoPt_3$ films grown on Pt(111) [4]. In this paper we describe the magnetic properties of $CoPt_3$(111) thin films deposited at room temperature on WSe_2(0001) as a function of film thickness.

EXPERIMENT

$CoPt_3$(111) films were grown by molecular beam epitaxy through the co-evaporation of Co and Pt from two e-beam sources at room temperature on WSe_2(0001) single crystals. The surface quality of the substrate was extremely high, showing atomically flat terraces with widths of several microns, as verified by scanning tunneling microscopy (STM). The Co and Pt atomic fluxes gave deposition rates of 0.001 and 0.0043 nm/s, respectively. Film thicknesses were controlled by a quartz-crystal balance and a quadrupole mass spectrometer. Structural characterization was performed by using in-situ reflection high energy electron diffraction (RHEED) and high-resolution x-ray diffraction (XRD). The results from these structural studies are reported elsewhere [5]. The magnetic properties of these films were measured by superconductive quantum interference device (SQUID) and photoemission electron microscopy (PEEM) using the PEEM-2 endstation at beamline 7.3.1. of the ALS [7]. Using monochromatized circularly polarized x-rays and applying x-ray magnetic circular dichroism (XMCD) as the contrast mechanism it is possible to obtain images showing the magnetic state of the sample. Images were acquired at the L_2 and L_3 edges of Co using circularly polarized x-rays incident at the sample at an angle of 30 degrees from the surface. The images were scaled to the same intensity and divided to eliminate topographic contrast and obtain only magnetic contrast.

RESULTS AND DISCUSSION

A series of $CoPt_3(111)$ samples deposited at room temperature with film thicknesses t of 3, 6, and 9 nm were produced. In order to protect the samples against oxidation an additional 2nm thick cap layer of vanadium was deposited. The morphology of these films, investigated by atomic force microscopy, consisted of a dense nanometer-sized grain structure. The average lateral dimension increased from 3nm to 6nm as the film thickness increased from 3 to 9nm. The averaged roughness over the whole surface was estimated to be in the range of up to 0.5nm [5].
We investigated the reorientation of the magnetization from perpendicular to in-plane as a function of film thickness in the range 3 to 9nm using SQUID at room temperature with the field applied either perpendicular or parallel to the plane of the film. The magnetization curves obtained for the 3nm thick $CoPt_3(111)$ film are characteristic of a film with perpendicular anisotropy with a squareness of S=1, a coercivity of 200Oe, a saturation magnetization of M_s=520emu/cm^3 and an effective anisotropy energy of $K_{eff}=1.5x10^6$erg/cm^3. We observed that effective anisotropy energy is reduced considerably by increasing the film thickness. At a film thickness larger than 6nm the easy magnetization axis rotates progressively into the film plane and K_{eff} changes sign.
Strong changes in anisotropy conditions are also reflected in the magnetic domain structure. The domain structure of films exhibiting perpendicular anisotropy was imaged by PEEM. It is worth mentioning that no magnetic contrast was found by magnetic force microscopy (MFM) due to the fact that the magnetic stray field from the MFM tip causes magnetization of the samples to change during the scanning process. Using circularly polarized x-rays and applying x-ray magnetic circular dichroism (XMCD) as the contrast mechanism we obtained images showing the magnetic state of the samples. All images reveal dark and white domains with only two different gray levels as shown in Fig. 1. This and the fact that the contrast of the image does not change when the sample is rotated in-plane are a clear indication that the direction of magnetization in those domains is perpendicular to the surface.

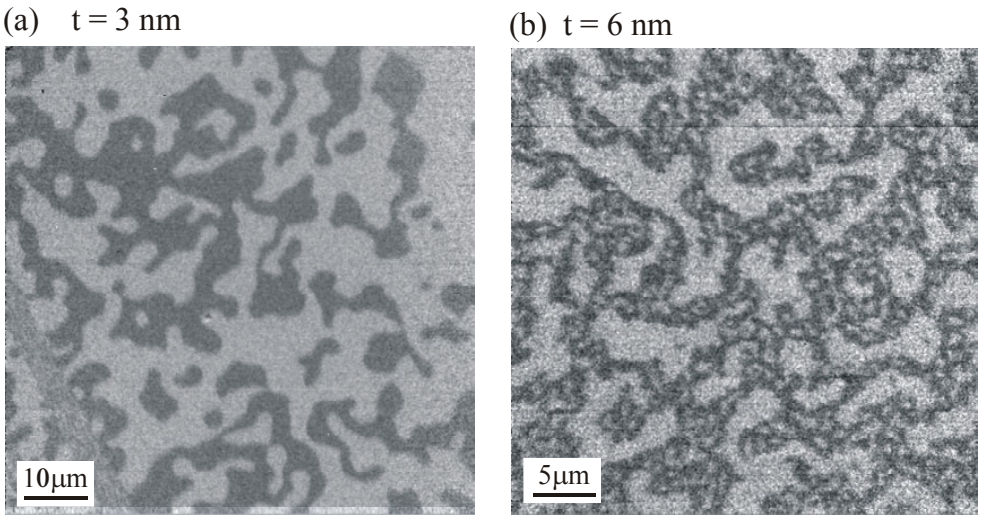

Figure 1. Perpendicular magnetic domain structures of $CoPt_3(111)$ films previously demagnetized out-of-plane with thicknesses (a) 3nm and (b) 6nm obtained by PEEM using XMCD contrast at the Co $L_{2,3}$ edges.

Prior to measurement the samples were demagnetized by exposing the sample to an alternating perpendicular magnetic field with decreasing amplitude, however a small net magnetization remained. The perpendicular domain structures can be characterized as one of two different

types. At a film thickness of 3nm we found a domain structure that appears serpentine in nature (Fig. 1(a)). Increasing the film thickness from 3 to 6nm (Fig.1(b)) the averaged domain size decreases from about 8 to 3microns. This decrease at a thickness near the onset of transition to in-plane magnetization is predicted by the theory of domain formation in thin perpendicular films. It is due to the fact that the magnetization can remain perpendicular by decreasing the shape energies via domain creation. In addition, nucleation of magnetic bubbles in the submicron length scale with opposite magnetization starts to fragment the larger domain features. This interior bubble domain structure also leads to a reduction of the magnetostatic energy inside a large domain and is therefore an energetically favorable process.

CONCLUSIONS

It is well known that in thin films growth (particularly for compounds) the choice of the substrate is important because it influences several properties such as surface mobility, growth mode, lattice parameter mismatch, and symmetry. Here we used a special substrate that has a van der Waals surface. On this surface single-crystal growth of (111)-oriented fcc $CoPt_3$ films was obtained even at room temperature. These films show strong perpendicular magnetic anisotropy for a thickness range of up to 6nm combined with an extremely small grain structure and are therefore potentially interesting as data storage media. For larger thicknesses a rotation of the magnetization from perpendicular to in-plane is observed. This reorientation is associated with a change in the magnetic domain structure observed by PEEM. We conclude that in the ultrathin film limit the strong perpendicular anisotropy is induced by some kind of thickness-dependent short-range ordering effects enhanced by the nanometer-sized film morphology. The change of anisotropy is connected with the diminution of short-range ordering as the film morphology changes from a isolated nucleation structure to a continuous material.

ACKNOWLEDGMENTS

The authors wish to thank Dr. U. Probst and Prof. Dr. E. Bucher (University of Konstanz, Germany) for providing single crystal substrates.

REFERENCES

1. D. Weller, H. Brändle, G.L. Gorman, C.J. Lin, H. Notarys, Appl. Phys. Lett. **61**, 2726 (1992).
2. D. Weller, H. Brändle, and C. Chappert, J. Magn. Magn. Mater. **121**, 461 (1993).
3. C. Meneghini, M. Maret, V. Parasote, M.C. Cadeville, J.L. Hazemann, R. Cortes, and S. Colonna, Eur. Phys. J. B **7**, 347 (1999).
4. A.L. Shapiro, P.W. Rooney, M.Q. Tran, F. Hellman, K.M. Ring, K.L. Kavanagh, B. Rellinghaus, and D. Weller, Phys. Rev. B **60**, 12826 (1999).
5. A. Maier, B. Riedlinger, F. Treubel, M. Maret, R. Poinsot, M. Albrecht, and G. Schatz, J. Magn. Magn. Mater. in print.
6. M. Maret, A. Maier, B. Riedlinger, F. Treubel, M. Albrecht, E. Beaurepaire, and G. Schatz, J. Magn. Magn. Mater. in print.
7. S. Anders, H.A. Padmore, R.M. Duarte, T. Renner, and M. Scheinfein, J. Stöhr, L. Séve, B. Sinkovic, Rev. Sci. Instrum. **70**, 3973 (1999).

We gratefully acknowledge financial support of this project from the Deutsche Forschungsgemeinschaft (DFG). This work was supported by SFB 513 at the University of Konstanz.
Principal investigator: Simone Anders, IBM Almaden Research Center, 650 Harry Road, San Jose CA 95120.
Email: simone@almaden.ibm.com. Telephone: 408-927-2069.

Photoemission Electron Microscopy and X-Ray Magnetic Circular Dichroism of $Fe_xNi_{(1-x)}$ Thin Films on Cu(111)

Y.Sato[1], T.F.Johnson[1], S.Chiang[1], X.D.Zhu[1], D.P.Land[2], J.A.Giacomo[1]
F.Nolting[3], and A.Scholl[3]

[1]Dept. of Physics, University of California, Davis, CA 95616
[2]Dept. of Chemistry, University of California, Davis, CA 95616
[3]Advanced Light Source, Lawrence Berkeley National Laboratory,Berkeley, CA 94720

INTRODUCTION

Our research focuses on controlling the structure, composition and the resultant magnetic properties of metal alloy thin film growth at the atomic level. Better understanding and control of surface/interface magnetism is relevant to the application of the giant magneto-resistive effect to read heads for magnetic recording. We have studied $Fe_xNi_{(1-x)}$ alloy thin films for their technological relevance to the above mentioned technology. The dependence of the magnetism on the stoichiometry x is one of the questions of interest. In addressing this problem, the structure of the thin film must be also considered. In terms of crystal structure, a well known "Invar effect" exists in bulk FeNi alloy because of structural incompatibilities of the two elements. Pure Fe is stable in bcc phase whereas pure Ni has fcc structure. A bulk alloy containing more than 65% Fe transforms to bcc by a Martensitic transformation, and the magnetization falls to zero. In thin film alloys, the problem may become more complex because of the effect of substrate structure and interface properties. On the other hand, how this structural change affects the magnetic order in the film is not well known. A simultaneous study of film structure, magnetic structure and magnetism is needed to better understand the system.

Several studies on $Fe_xNi_{(1-x)}$ alloy thin films have been reported[1,2,3,4]. Information on the growth, structure, and magnetic moments as a function of thickness and concentration has been obtained using various techniques such as low energy electron diffraction (LEED), reflection high energy electron diffraction (RHEED), photoelectron diffraction, surface magneto optical Kerr effect (SMOKE), X-ray magnetic linear dichroism (XMLD), Mossbauer spectroscopy, and superconducting quantum interference device (SQUID) magnetometry. We have used the photoemission electron microscope (PEEM2) at the Advanced Light Source (beamline 7.3.1.1) to study this film system. PEEM has the unique capability of imaging the film's magnetic structure with high spatial resolution and elemental specificity. Simultaneously, quantitative magnetic information can be obtained using magnetic circular dichroism in X-ray absorption spectroscopy. At two different thicknesses, we have made sixteen samples and studied the dependence of magnetic structure on varying Fe concentration and substrate quality (x = 0, 0.28, 0.55,0.6, 0.66, 0.74, 1.0 at 10Å≅5ML, x = 0.9, 0.25, 0.33, 0.42, 0.5, 0.55, 1.0 at 20Å ≅10ML). We have observed clear ferromagnetic domain structures of the film on a Cu(111) surface for $x \leq 0.60$ at room temperature.

RESULTS

Samples with high Fe content (x=0.66, 0.74 at 5ML) have been observed to be non-magnetic at room temperature. All other alloy samples ($x \leq 0.6$, 5ML and 10ML) showed clear ferromagnetic contrast. This trend of reduction in Curie temperature at higher Fe concentration is also observed by spin resolved photoemission spectroscopy measurements carried out at the Advanced Light Source (beamline 7.0.1.2). A pure Ni film at 5ML thickness was non-magnetic at room temperature. According to a SMOKE measurement, 5ML is approximately the thickness where the Curie temperature becomes less than room temperature for Ni/Cu(111)[5].

Fig. 1 shows typical ferromagnetic images with a 12μ m field of view for a 5ML thick $Fe_{0.6}Ni_{0.4}$ film on Cu(111). Each image is obtained by dividing an image acquired at the L3 Fe (or Ni) edge by one acquired at the L2 Fe (or Ni) edge. The images show alignment of the magnetic domains for

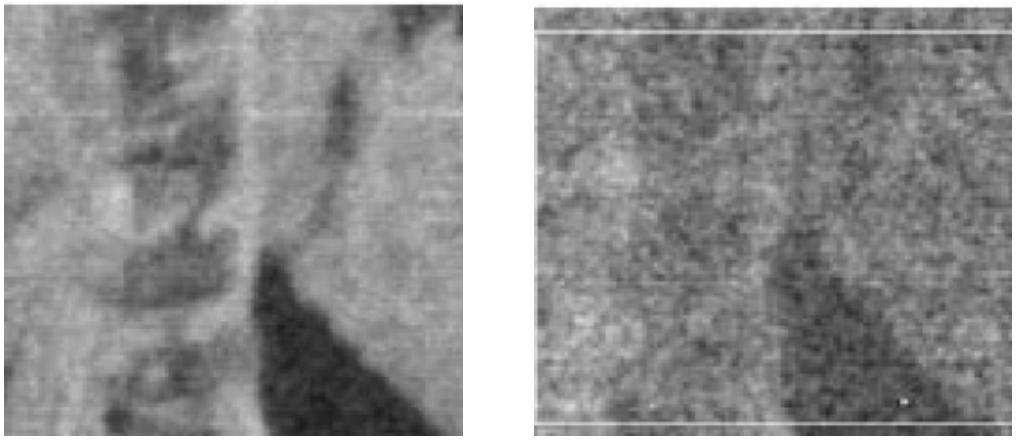

Fig. 1. XMCD ferromagnetic images with a 12μ m field of view for a 5ML thick $Fe_{0.6}Ni_{0.4}$/Cu(111). Left: Fe XMCD contrast, Right: Ni XMCD contrast.

Fe and Ni, suggesting that Fe and Ni form a good alloy on this surface. By comparing the images shown in Fig. 2 and Fig. 3, we find a clear dependence of the domain structures on film thickness and substrate quality. Fig. 2 shows magnetic contrast images of 5ML alloy films on a mechanically polished substrate. On these samples, observed magnetic structures appear to correlate to surface topographic features. No regular apperance of domain structure was seen. Comparison of the image at the pre-absorption edge, which shows only topographic contrast, with the magnetic contrast image clearly shows the correlation between surface structural features and the formation of magnetic domains. An experiment showed that magnetic contrast observed at room temperature disappears gradually upon heating. Contrast is recovered again as the sample temperature is lowered below the Curie temperature. This also confirms the relation between domain structure and surface geometric structures. These observations are consistent for each 5ML sample analyzed. In contrast, for 10ML films on an electropolished substrate as shown in Fig. 3, pinning due to surface defects is observed less frequently. Magnetic structures and textures appear to be more uniform and the sizes of the structures were smaller and on the order of 1-3μ m. At the alloy composition of x=0.44, regular, periodic appearance of larger domain structures (5-10μ m width and 70μ m length), defined by 180º domain walls, are observed, as shown in Fig. 4. By observing the two images shown in Fig. 4, we conclude that alloy film at this composition and thickness show in-plane magnetization.

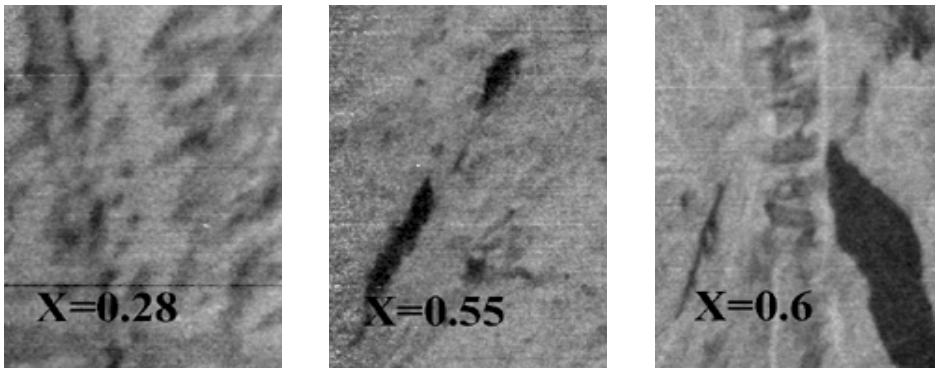

Fig. 2. XMCD ferromagnetic images with H22μ m×V30μ m field of view for 5ML films with varying Fe composition x.

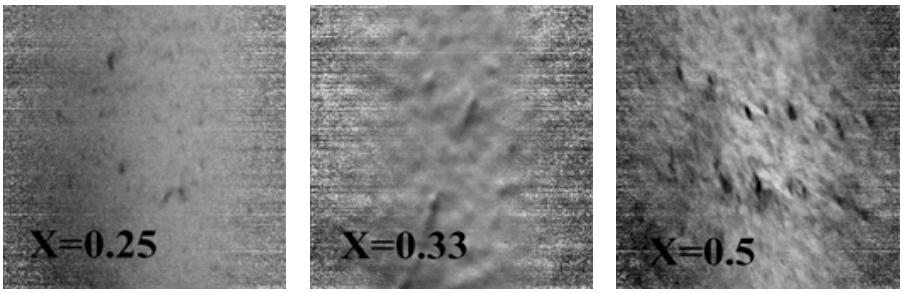

Fig. 3. XMCD ferromagnetic images with H65μ m×V65μ m field of view for 10ML films with varying Fe composition x.

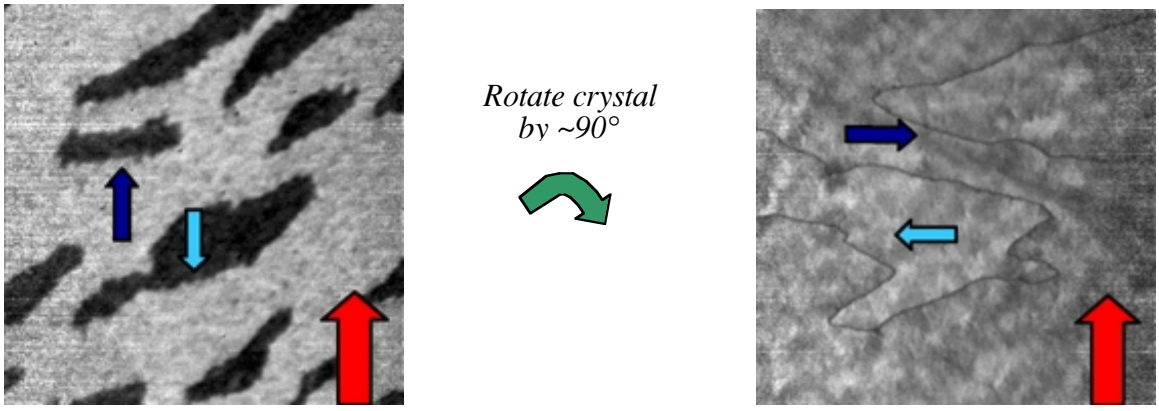

Fig. 4. XMCD ferromagnetic images with Right: H45μ m×V45μ m and Left: H45μ m×V45μ m field of view for 10ML thick $Fe_{0.56}Ni_{0.44}$/Cu(111). Smaller arrows indicate the magnetization direction and larger arrows show the direction of the incident photon momentum.

REFERENCES

1. F.O.Schumann, S.Z.Wu, G.J.Mankey, and R.F.Willis *Phys. Rev. B* **56** 2668 (1997)
2. F.O.Schumann, R.F.Willis, K.G.Goodman, and J.G.Tobin *Phys. Rev. Lett.* **79** 5166 (1997)
3. J.W.Freeland, I.L.Grigorov, and J.C.Walker *Phys. Rev. B.* **57** 80 (1998)
4. R.Schellenberg, H.Meinert, N.Takahashi, F.U.Hillebrecht, and E.Kisker *J. App. Phys.* **85** 6214 (1999)
5. R.Zhang, and R.F.Willis *Phys. Rev. Lett.* **86** 2665 (2001)

This work was supported by the Campus Laboratory Collaboration Program of the University of California Office of the President and by the Director, Office of Energy Research, Office of Basic Energy Sciences, of the U.S. Department of Energy under Contract No. DE-AC03-76SF00098.

Principal investigator: Shirley Chiang, Department of Physics, University of California, Davis, CA 95616-8677. Email: chiang@physics.ucdavis.edu. Telephone: 530-752-8538.

Soft X-ray absorption spectroscopy of *single* nanocrystals

F. Nolting[1,2,5], J. Rockenberger[3,4], J. Lüning[2], J. Hu[3,4], and A. P. Alivisatos[3,4]
[1]Advanced Light Source, Ernest Orlando Lawrence Berkeley National Laboratory, Berkeley, CA 94720, USA
[2]Stanford Synchrotron Radiation Laboratory, Stanford, CA 94309, USA
[3]Universtiy of California at Berkeley, Department of Chemistry, Berkeley, CA 94720, USA
[4]Lawerence Berkeley National Laboratory, Materials Science Division, Berkeley, CA 94720, USA
[5]Swiss Light Source, Paul Scherrer Institut, 5232 Villigen PSI, Switzerland

INTRODUCTION

A common limitation in nanostructure research is often the requirement to perform experiments on ensembles of nanoparticles, therefore averaging over inherent distributions with respect to particle size and shape, chemical composition, crystallinity and defect structure. This limitation can be overcome by studying the properties of a single nanostructure individually, which will allow to truly correlate scaling laws of material properties with changes in size. Here, we demonstrate the applicability of spatially resolved Photoemission Electron Microscopy (PEEM) to measure soft x-ray absorption spectra at the Fe $L_{3,2}$ edges of *single* colloidal iron oxide nanocrystals with an average diameter of 10 nm (~ 20,000 iron atoms). The experiment was carried out with the PEEM2 instrument of the ALS [1]. Details of the experiment can be found in [2,3].

EXPERIMENT

Surfactant-capped nanocrystals of γ-Fe_2O_3 (maghemite) were prepared by a slightly modified version of a recently published procedure using hexadecylamine as surfactant [4]. A fraction was isolated by repeated size-selective precipitation using methanol as precipitating agent and the average particle size was determined by TEM to be 10 nm with a standard deviation of 3 nm. Very dilute toluene solutions of this sample were spin-coated onto silicon wafers that were freshly cleaned by etching with HF and washing with deionized H_2O. The particle coverage of the silicon substrate was determined by high-resolution Scanning Electron Microscopy (SEM) at the National Center for Electron Microscopy, Lawrence Berkeley National Laboratory. From the relative positions of the particles in the SEM images (Fig 1A), a mean first nearest neighbor distance of 485 nm was derived. This is sufficiently larger than the spatial resolution of the PEEM microscope in this study. In contrast to our fist study [2,5] using graphite as substrate, we were never able to resolve these spots into smaller aggregates indicating that they, indeed, represent individual nanocrystals. Also, linescans through individual spots show FWHM in the range of 8 – 15 nm in good agreement with the particle size distribution of the sample as determined by TEM.

The PEEM experiments were performed at the bending magnet beamline 7.3.1.1 of the ALS. The best lateral spatial resolution achieved by PEEM to date is about 20 nm, but it depends strongly, in addition to the settings of the instruments, on the topography and conductivity of the sample. In the studies presented here, the spatial resolution was about 150 nm. Fig. 1B shows a chemical contrast image which was obtained by subtracting an image taken at a pre-edge photon energy (700 eV) from the one taken at the iron L_3 edge (707 eV). Hence, the bright spots indicate the presence of iron oxide nanocrystals. The varying brightness of the spots is most likely related to the rather broad size distribution of the iron oxide nanocrystals in the sample with an average diameter and a standard deviation of 10 nm and 3 nm, respectively. In Fig. 1C, the local x-ray absorption spectra of a location appearing bright in Fig 1B (area I) is compared to the one of a dark area (area II). As expected, the spectrum of the bright spot (area I) shows the signature of the Fe L_3 absorption edge

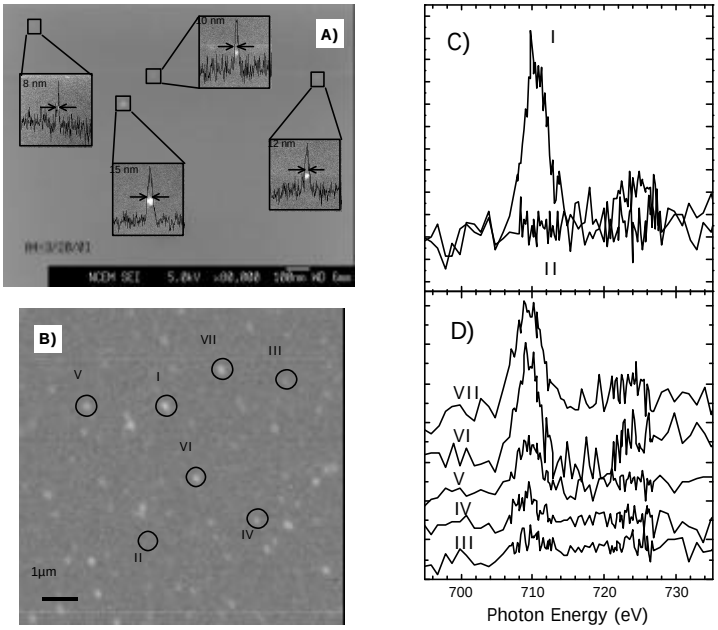

Figure 1: a) High-magnification SEM image of γ-Fe_2O_3 nanocrystals deposited onto Silicon wafer. B) PEEM chemical contrast image. C) Spatially resolved X-ray absorption spectrum recorded in a bright area (I) and a dark area(II). D) Local spectra for different bright spots in b).

at 707 eV, whereas the dark background (area II) shows no detectable structure of the absorption intensity in this energy range. Due to the moderate energy resolution, the multiplet structure of the typical x-ray absorption spectra of Fe^{3+}-ions at the L_3-edge is not resolved. In Fig. 1D, the x-ray absorption spectra of several positions with varying intensities in Fig. 1B (areas III - VII) are compared. Clearly, even in cases with very small intensity in the contrast image in Fig. 1B the Fe L_3 x-ray absorption edge is still discernible from the background whereas the weaker L_2 edge is only barely recognizable. We emphasize that these spectra indeed reflect the x-ray absorption spectra of individual particles with diameters of (10 ± 3) nm with a small chance that some spectra are due to the presence of dimers or trimers of particles (< 13%) [3]. To the best of our knowledge, this represents the first time that soft x-ray absorption spectra of individual nanocrystals at this length scale are reported [6].

This work was supported by the Director, Office of Basic Energy, Division of Chemical Sciences and the Division of Materials Sciences of the U.S. Department of Energy, the Air Force Office of Scientific Research, and the Deutsche Forschungsgemeinschaft.
Principal investigator: Frithjof Nolting. Email: frithjof.nolting@psi.ch. Telephone: +41 56 310 5111.

REFERENCES

[1] S. Anders, *et al*., Rev. Sci. Instrum. **70**, 3973 (1999).
[2] F. Nolting, J. Lüning, J. Rockenberger, J. Hu, and A. P. Alivisatos, Surf. Rev. Lett. (2002), accepted.
[3] J. Rockenberger, F. Nolting, J. Lüning, J. Hu, A. Paul Alivisatos, J. Chem. Phys. (2002), accepted.
[4] J. Rockenberger, E. C. Scher, and A. P. Alivisatos, J. Am. Chem. Soc. **121,** 11596 (1999).
[5] F. Nolting, J. Rockenberger, J. Lüning, Jiangtao Hu, and A. Paul Alivisatos, ALS Compendium, 2000, LBNL publication, 47838.
[6] Recently, x-ray photoemission spectra of InAs nanocrystals were reported by Heun et al., Phys. Rev. B **2001**, *63*, 125335. They presented averages spectra over all InAs nanocrystals imaged. Also, the InAs nanocrystals with an average diameter and height of 55 nm and 22 nm, respectively, contain significantly more atoms (factor of 40) than the 10 nm γ-Fe_2O_3 nanoparticles investigated here.

Valence-state imaging of mineral micro-intergrowths

A.D.Smith[1], P.F.Schofield[2] and A.Scholl[3]

[1]CLRC Daresbury Laboratory, Daresbury, Warrington Cheshire, WA4 4AD United Kingdom
[2]Department of Mineralogy, The Natural History Museum, London, SW7 5BD United Kingdom
[3]Advanced Light Source, Ernest Orlando Lawrence Berkeley National Laboratory,
University of California, Berkeley, California 94720, USA

INTRODUCTION

The crystal chemistry and textural relationships of minerals hold a vast amount of information relating to the formation, history and stability of natural materials. An understanding of the detailed crystal chemistry of minerals within rocks, meteorites, soils, sediments, mineral-fluid/biota interfaces etc. will ultimately develop both an understanding of the processes involved with their formation and also a knowledge of their properties, reactivity and stability within their current environment. The acquisition of such knowledge is, however, non-trivial, due in no small part to the vast array of textural relationships and mineral assemblages observed, combined with their polygenetic history.

Minerals generally comprise complex structures with large unit cells that contain complex and varied crystal chemistries. For example, the 3d transition metals impart a significant influence on mineral properties and behaviour, existing at major, minor and trace concentrations and also exhibiting multiple valence states. Knowledge of the valence state ratios of these metals within minerals and mineral assemblages is fundamental to the calculation of geochemical variables such as pressure, temperature and oxygen fugacity. The application of soft X-ray spectroscopy to mineralogical material has revealed that 2p($L_{2,3}$) spectra provide a sensitive fingerprint of the electronic states of 3d metals [1-4]. In bulk powdered samples much of the textural and microstructural information is lost, but the area-selectivity capability of X-ray Photo-Emission Electron Microscopy (XPEEM) provides the ability to obtain valence state information from mineral intergrowths with a submicron spatial resolution [5,6,7].

RESULTS

Sulphide Intergrowths

Pentlandite, $(Fe,Ni)_9S_8$, is the primary sulphide ore of Ni and usually occurs intergrown with the iron sulphide pyrrhotite, FeS. Figure 1 shows data obtained using the PEEM2 beamline at ALS and reveals the high quality of imaging and XAS data that can be obtained from XPEEM. The left hand image has an estimated field of view < 20μm and was taken at 715.0eV, the main feature of the FeS pyrrhotite Fe $L_{2,3}$ spectrum. It thus shows the distribution of Fe in the chemical state equivalent to that of Fe in pyrrhotite. The light grey areas represent Fe from pyrrhotite, whereas the dark grey regions represent the Fe in pentlandite. The Fe $L_{2,3}$ spectrum below the image has been collected from the full image area. XPEEM allows an area selectivity such that an Fe $L_{2,3}$ spectrum can be obtained from any area of the image, thus providing a spatial resolution in the order of 0.1μm. The right hand image, with an estimated field of view < 40μm, is taken at 864.5eV the main feature of the $(Fe,Ni)_9S_8$ pentlandite Ni $L_{2,3}$ spectrum and the Ni $L_{2,3}$ spectrum from the whole image is below this image. Close investigation has shown banding of nickel and iron, with possible variations in the chemical state of the iron, in the ‘feathers’ of the pentlandite on a sub 200nm scale.

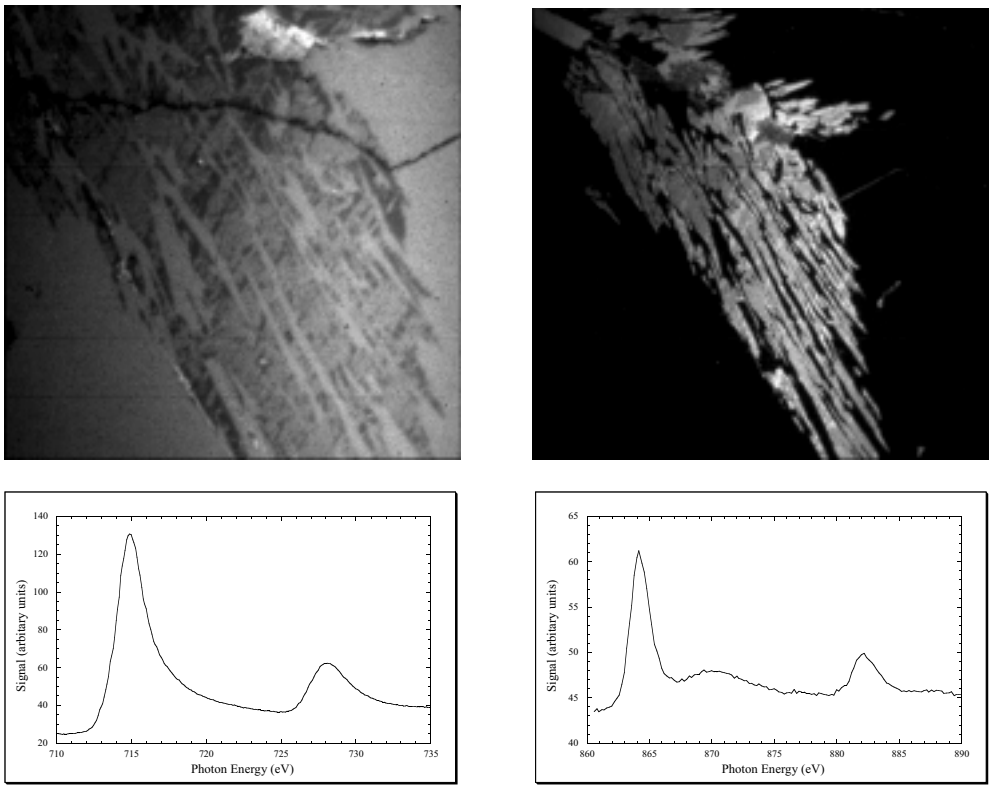

Figure 1. PEEM2 images from a pentlandite/pyrrhotite intergrowth. The left hand image is taken at 715.0eV – the main feature of the Fe L_{23} spectrum (below), and the right hand image was recorded at 864.5eV – the principal feature of the Ni L_{23} spectrum (below).

Hydrothermal Vent Sediments

Sulphide-to-oxide alteration behaviour in sea-floor hydrothermal vent samples recovered from the North Atlantic may potentially be observed from metal and sulphur valence information on a microscopic length scale. Mn^{2+}/ Mn^{3+}/ Mn^{4+} ratios as well as Fe^{3+}/Fe^{2+} are likely to be related to the extent of sulphate-reducing bacteria active at different horizons in these recent sea-floor hydrothermal deposits. Little is known about the micro-ecology in which these bacteria live, however it is thought that they are able to substantially modify their environment due to large differences observed in the redox conditions of various minerals contained in different strata of sea floor cores. Figure 2 shows iron, copper and oxygen chemical state images in a sample taken from the sediment around an active hydrothermal vent on the mid-Atlantic ridge. The unconsolidated sediment has been embedded in epoxy resin, sliced and polished but still provides excellent images and $L_{2,3}$ spectra.

The PEEM2 images show clear growth features that may reflect differing environments, oxidizing conditions and micro-ecologies. The top images show alternating Cu and Fe growth rings on the submicron scale indicating a low oxygen environment. The lower images show a submicron thick, copper sulphide precipitate that has grown around an iron sulphide grain. This ring represents both a different source fluid and a more reduced environment to that of the bulk Fe-oxides present in the image.

ACKNOWLEDGEMENTS

This work was funded by the UK ENVIROSYNCH project and the authors are grateful to Professor C.M.B. Henderson and Dr J.F.W. Mosselmans for the provision and management of

this project. Beamtime at ALS was awarded under project code ALS-548. The assistance of Hendrik Ohldag and Andrew Doran on the PEEM2 beamline is also greatly appreciated.

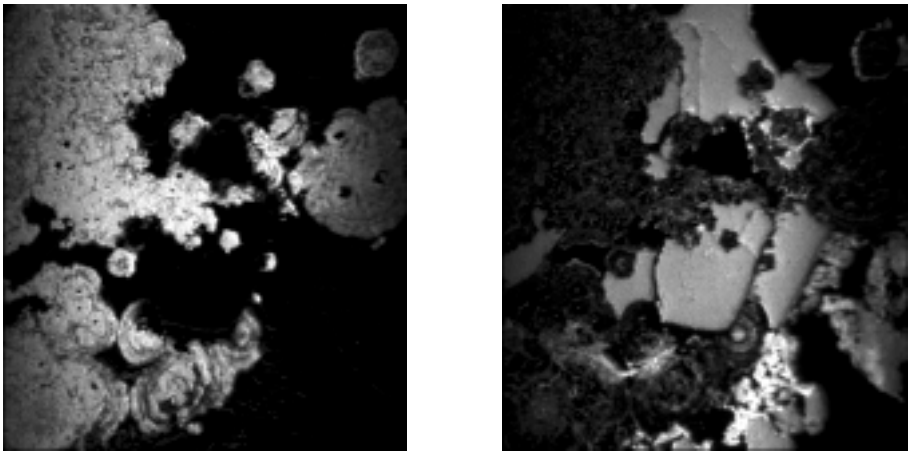

Figure 2. PEEM2 chemical state images from a sediment associated with a mid-Atlantic ridge hydrothermal vent. The top images are Cu (left) & Fe (right) and have a field of view of <30μm and reveal clear botryoidal textures or growth features that may be related to bacterial micro-ecological cycles. The lower images are Fe (left), Cu (middle) & O (right) and have a field of view of <20μm. The Cu 'ring' appears to be a sulphide precipitate with a thickness of about 0.5<30μm that has grown around an Fe sulphide grain. The majority of the Fe phases in these images are clearly oxidized

REFERENCES

[1] Cressey G. et al. (1993) Physics and Chemistry of Minerals 20 pp111-119
[2] Henderson C.M.B. et al. (1995) Radiation Physics and Chemistry 45 pp459-481
[3] Schofield P.F. et al. (1995) Journal of Synchrotron Radiation 2 pp93-98
[4] van der Laan G. and Kirkman I.W. (1992) Journal of Physics: Condensed Matter 4 pp4189-4202
[5] Smith A.D. et al. (1998) Journal of Synchrotron Radiation 5 pp1108-1110
[6] Cressey G. et al. (1998) 17th General Meeting, International Mineralogical Association, A128
[7] Smith A.D. et al. (1999) ALS Compendium 1997/8

Principal investigator: A.D. Smith, CLRC, Daresbury Laboratory. Telephone: 44-1925-603314.
Email: a.d.smith@dl.ac.uk.